Adjustment to Radiative Forcing In a Simple Coupled Ocean-Atmosphere Model

R. L. Miller*

NASA Goddard Institute for Space Studies, New York, USA

Department of Applied Physics and Applied Math, Columbia University, New York, USA

* *Corresponding author address:* R. L. Miller, NASA Goddard Institute for Space Studies, 2880 Broadway, New York, NY 10025.

E-mail: rlm15@columbia.edu

ABSTRACT

We calculate the adjustment to radiative forcing in a simple model of a mixed-layer ocean coupled to the overlying atmosphere. One application of the model is to calculate how dust aerosols perturb the temperature of the atmosphere and ocean, which in turn influence tropical cyclone development. Forcing at the top of the atmosphere (TOA) is the primary control upon both the atmospheric and ocean temperature anomalies, both at equilibrium and during most of the adjustment to the forcing. Ocean temperature is directly influenced by forcing only at the surface, but is indirectly related to forcing at TOA due to heat exchange with the atmosphere. Within a few days of the forcing onset, the atmospheric temperature adjusts to heating within the aerosol layer, reducing the net transfer of heat from the ocean to the atmosphere. For realistic levels of aerosol radiative forcing, the perturbed net surface heating strongly opposes forcing at the surface. This means that surface forcing dominates the ocean response only within the first few days following a dust outbreak, before the atmosphere has responded. This suggests that to calculate the effect of dust upon the ocean temperature, the atmospheric adjustment must be taken into account explicitly, and forcing at TOA must be considered in addition to the surface forcing. The importance of TOA forcing should be investigated in a model where vertical and lateral mixing of heat are calculated with fewer assumptions than in the simple model presented here. Nonetheless, the fundamental influence of TOA forcing appears to be only weakly sensitive to the model assumptions.

1. Introduction

Where the atmosphere is mixed vertically, radiative forcing at the top of the atmosphere (TOA) has a greater influence upon the surface air temperature than forcing at the surface. This is because the atmosphere balances TOA forcing by adjusting outgoing longwave radiation (OLR), and most longwave radiation to space originates in the upper troposphere due to the longwave opacity of the air below. OLR depends strongly upon the upper tropospheric temperature, and because of vertical mixing of heat by deep convection, variations in temperature at this level lead to corresponding adjustments of the surface air temperature. The primary importance of TOA forcing to climate at the surface has long been recognized (e.g. Cess et al. 1985). For this reason, the climate effect of atmospheric constituents like greenhouse gases is often characterized by their radiative forcing at TOA (e.g. Forster et al. 2007).

The primacy of TOA forcing is illustrated by the response to dust radiative forcing in a general circulation model (Miller and Tegen 1998). Over the Arabian Sea during Northern Hemisphere (NH) summer, surface air temperature is virtually unchanged beneath a dust layer, consistent with the small aerosol forcing at TOA. The unperturbed temperature occurs despite strong negative forcing at the surface approaching $70\,\mathrm{Wm}^{-2}$ in magnitude. The surface forcing is mainly balanced by a reduction in evaporation, affected by a reduction in the sea-air temperature difference through cooling of the ocean by a few tenths of a degree K. In another model with strong negative forcing at the surface, surface air temperature actually increases when the forcing at TOA is positive (Miller and Tegen 1999).

Sea surface temperature (SST) is directly related to forcing at the surface, because the latter is a component of the surface energy budget. However, TOA forcing influences SST indirectly by perturbing the surface air temperature, which is coupled to SST through the turbulent exchange of latent and sensible heat along with net longwave radiation. These surface fluxes keep SST close to the surface air temperature so that at equilibrium, TOA forcing also has a primary influence on SST (e.g. Pierrehumbert 1995). However, after the onset of radiative forcing, there is a period before the atmosphere has adjusted, when SST is influenced mainly by radiative forcing at the surface. In this article, we calculate the time-evolution of the ocean and atmospheric temperature to radiative forcing using a simple model proposed by Schopf (1983). We describe the transition between the initial period when SST adjusts to the surface radiative forcing, and the longer adjustment as the surface turbulent and longwave fluxes eventually bring SST and the atmospheric temperature into equilibrium with forcing at TOA. Our model shows that the initial influence of the surface forcing is limited to roughly a week and that forcing at TOA controls the magnitude of the SST anomaly over almost the entire duration of the adjustment. Our model also illustrates how the ocean comes into balance with the surface forcing, even though SST and surface air temperature are fundamentally controlled by forcing at TOA.

One application of the model is to calculate the reduction of SST by aerosols, which in turn could influence tropical cyclones. Tropical cyclone activity in the North Atlantic is smaller during dusty years (Evan et al. 2006), when wind erosion over African deserts leads to unusually large amounts of soil dust particles transported offshore within the Saharan Air Layer (SAL) (Carlson and Prospero 1972). One hypothesis is that dust inhibits tropical cyclones by cooling the ocean through a reduction in radiation reaching the surface beneath the aerosol layer (Lau and Kim 2007b). This hypothesis has been tested in two ways. First, the SST anomaly measured or retrieved by satellite is regressed against aerosol optical thickness (AOT) or some measure of the aerosol forcing following a dust outbreak (e.g. Schollaert and Merrill 1998; Foltz and McPhaden 2008a; Martińez Avellaneda et al. 2010). This attribution is challenging because of other sources of SST variability: for example, clouds. An additional difficulty is that SST adjusts over a time scale of several months that encompasses multiple outbreaks, so that the relation between anomalies of SST and AOT that are simultaneous or separated by short lags may not reveal the true sensitivity. Alternatively, the hypothesis is tested by calculating the SST anomaly that results from the estimated forcing at the surface, and comparing its magnitude to that of observed SST variations (e.g. Lau and Kim 2007a; Evan 2007; Lau and Kim 2007c; Foltz and McPhaden 2008b,a; Evan et al. 2008, 2009; Martińez Avellaneda et al. 2010). This SST anomaly is calculated using an energy budget for the ocean mixed layer. In this article, we argue that the turbulent and longwave fluxes at the surface are an important feedback upon SST following surface radiative forcing by dust, and that these fluxes depend upon the atmospheric state. Dust radiative forcing at TOA thus must be accounted for in the calculation of SST, due to the influence of forcing at this level upon the surface air temperature.

In Section 2, we describe the simple model of Schopf (1983) used to investigate the comparative influence of radiative forcing at the surface and TOA upon the evolution of atmospheric and ocean temperature anomalies. In Section 3, we calculate unforced solutions that contribute to the temperature adjustment. The time-dependent, forced response of temperature to aerosol radiative forcing is presented in Section 4. In Section 5, we examine some of the assumptions used to construct our model and their effect upon model behavior. Our conclusions are presented in Section 6, along with their implication for calculation of SST anomalies resulting from dust aerosols, and the interaction of dust with tropical cyclones.

2. Simple Coupled Model

We start with a model based upon Schopf (1983) that is illustrated schematically in Figure 1. The model consists of an atmosphere with surface pressure P_s over an ocean of depth h. Both layers are assumed to be well-mixed vertically so that temperature within each layer can be characterized by a value at a single level. The ocean layer is assumed to be stirred by the wind, while deep convection maintains a moist adiabatic lapse rate in the atmosphere. The main development region for Atlantic tropical cyclones is a region of active convection (Betts 1982). However, during NH summer, dust concentration is largest within the SAL, a duct of warm, dry air that is perched above the marine boundary layer due to its greater buoyancy acquired over the intensely heated Sahara desert. The vertical stability of the atmosphere increases during dust outbreaks, when dust radiative forcing is largest, and deep convection is temporarily suppressed by an unusually strong Trade Inversion (e.g. Dunion and Velden 2004; Wong and Dessler 2005). We will reexamine the assumption of a fixed lapse rate in Section 5.

In the absence of aerosol radiative forcing, solar radiation incident upon the surface is assumed to be balanced by ocean heat loss through a combination of turbulent fluxes of latent and sensible heat along with a net upward longwave flux. We assume that the ocean is warmer to allow this transfer of heat to the atmosphere. In response to aerosol forcing at the surface F_S, the ocean temperature anomaly T_O will adjust according to:

$$\rho h C_{p,o} \frac{\partial T_O}{\partial t} = k(T_A - T_O) - 4\sigma \bar{T}_O^3 T_O + \epsilon 4\sigma \bar{T}_A^3 T_A + F_S, \tag{1}$$

where ρ is the ocean density, and $C_{p,o}$ is the specific heat of seawater at constant pressure. In addition, T_A is the change in the atmospheric temperature due to aerosol forcing, σ is the Stefan-Boltzmann constant, $\bar{T}_O$ is the unperturbed temperature of the ocean mixed-layer, and $\bar{T}_A$ is the unperturbed temperature of the atmosphere whose longwave broadband emissivity is ϵ. On the right-hand side of (1), the first term represents the anomalous turbulent flux of latent and sensible heat that is approximated as proportional to the air-sea temperature difference. The terms $-4\sigma \bar{T}_O^3 T_O$ and $\epsilon 4\sigma \bar{T}_A^3 T_A$ represent the upward flux of longwave radiated by the ocean surface and the downward flux of atmospheric longwave, respectively. Eq. (1) assumes that T_O and T_A, the ocean and atmosphere temperature anomalies forced by dust, respectively, are small enough that the turbulent and longwave fluxes can be linearized.

The corresponding energy budget for the atmosphere is:

$$\frac{P_s}{g} C_{p,a} \frac{\partial T_A}{\partial t} = k(T_O - T_A) + 4\epsilon\sigma \bar{T}_O^3 T_O - 8\epsilon\sigma \bar{T}_A^3 T_A + (F_T - F_S). \tag{2}$$

Here P_s is the pressure difference between the top and bottom of the atmospheric column that is mixed by deep convection, g is acceleration by gravity, and $C_{p,a}$ is the specific heat of the atmosphere at constant pressure. On right hand side are the turbulent flux from the ocean to the atmosphere, heating by the absorption of longwave emitted by the ocean, cooling by the divergence of longwave emitted by the atmosphere, and heating of the atmospheric column by aerosols, equal to the difference in forcing between TOA (F_T) and the surface.

Our model has only vertical dependence and thus omits horizontal energy transport. The model is intended to interpret the relation between aerosol forcing and the ocean response in a specific region where tropical cyclones develop. The tropical atmosphere will adjust its temperature beyond the regional extent of the aerosol layer (Miller and Tegen 1999; Chou et al. 2005; Rodwell and Jung 2008). We will address the possible effect of dynamical adjustment upon the model behavior in Section 5.

We divide both equations by the total heat capacity of the ocean $\rho h C_{p,o}$, and define:

$$\tau_K \equiv \frac{\rho h C_{p,o}}{k},\ \tau_A \equiv \frac{\rho h C_{p,o}}{\epsilon 4\sigma \bar{T}_A^3},\ \tau_O \equiv \frac{\rho h C_{p,o}}{4\sigma \bar{T}_O^3},\ \text{and } \delta \equiv \frac{P_s}{\rho g h}\frac{C_{p,a}}{C_{p,o}}. \tag{3}$$

The parameters τ_K, τ_A, and τ_O are time scales representing the efficiency of heat exchange by the surface turbulent flux, along with longwave emission by the atmosphere and ocean, respectively. In Appendix A, we estimate numerical values based upon observations, and find that:

$$\tau_A \approx \tau_O \gg \tau_K. \tag{4}$$

That is, the radiative adjustment times of the ocean and atmosphere are comparable, but both are much longer than the time scale governing heat exchange between the atmosphere and ocean. Expressed in terms of these time scales, the equations for the evolution of the ocean and atmospheric temperature become:

$$\frac{\partial T_O}{\partial t} = \frac{1}{\tau_K}(T_A - T_O) + \frac{1}{\tau_A}T_A - \frac{1}{\tau_O}T_O + \frac{F_S}{\rho h C_{p,o}}, \tag{5}$$

and:

$$\delta\frac{\partial T_A}{\partial t} = \frac{1}{\tau_K}(T_O - T_A) + \frac{\epsilon}{\tau_O}T_O - \frac{2}{\tau_A}T_A + \frac{F_T - F_S}{\rho h C_{p,o}}. \tag{6}$$

Note that the tendency of atmospheric temperature is multiplied by δ, a small number representing the heat capacity of the atmospheric column compared to that of the ocean mixed layer. This ratio is small for two reasons. First, seawater has a heat capacity per unit mass roughly four times that of air. Second, the mass of an atmospheric column corresponds to about ten meters of seawater. In Appendix A, we estimate $\delta = 0.10$, given a mixed-layer depth of 20 m. Westward toward the Caribbean, the mixed layer may be several times deeper and δ is correspondingly smaller (de Boyer Montégut et al. 2004).

3. Unforced Solutions

We start by deriving unforced solutions to the coupled equations, because they contribute to the adjustment of the atmosphere and ocean to the new forced state.

To find the unforced (i.e. homogeneous) solutions, we set the forcing to zero, and because the remaining coefficients have no time dependence, we look for coupled solutions proportional to $\exp(-\lambda t)$. This requires finding the eigenvalues λ that satisfy:

$$\det \begin{vmatrix} \frac{1}{\tau_K} + \frac{1}{\tau_A} & -\frac{1}{\tau_K} - \frac{1}{\tau_O} + \lambda \\ -\frac{1}{\tau_K} - \frac{2}{\tau_A} + \delta\lambda & \frac{1}{\tau_K} + \frac{\epsilon}{\tau_O} \end{vmatrix} = 0$$

This leads to a quadratic in the product $\lambda\tau_K$:

$$\delta(\lambda\tau_K)^2 - \left[\delta\left(1 + \frac{\tau_K}{\tau_O}\right) + \left(1 + \frac{2\tau_K}{\tau_A}\right)\right](\lambda\tau_K) + \left[\frac{\tau_K}{\tau_A} + (1-\epsilon)\frac{\tau_K}{\tau_O} + (2-\epsilon)\frac{\tau_K^2}{\tau_A\tau_O}\right] = 0. \quad (7)$$

For small values of δ, we can forego the exact but unwieldy solution to (7) provided by the quadratic formula, and look instead at the approximate eigenvalues, whose physical interpretation is more transparent.

a. The Coupled (or 'Slow') Mode

For one solution to (7), the variations of the atmosphere and ocean are tightly coupled. We describe this solution as the 'coupled' eigenvalue, denoted by λ_c:

$$\lambda \equiv \lambda_c \approx \frac{\frac{\tau_K}{\tau_A} + (1-\epsilon)\frac{\tau_K}{\tau_O} + (2-\epsilon)\frac{\tau_K^2}{\tau_A\tau_O}}{\left(1 + \frac{2\tau_K}{\tau_A}\right)\tau_K}. \quad (8)$$

For an atmosphere that is opaque in the longwave (so that ϵ is near unity), the time scale λ_c^{-1} corresponding to the eigenvalue can be further approximated as:

$$\lambda_c^{-1} = \tau_A \left(\frac{1 + 2\frac{\tau_K}{\tau_A}}{1 + \frac{\tau_K}{\tau_O}} \right) \approx \tau_A = \frac{\rho h C_{p,o}}{4\sigma \bar{T}_A^3}, \tag{9}$$

where we have neglected terms of order $\frac{\tau_K}{\tau_A}$ and $\frac{\tau_K}{\tau_O}$ using (4). The eigenvalue corresponds to relaxation on a time scale that increases with the heat capacity of the ocean $\rho h C_{p,o}$, and decreases with the ability of the atmosphere to shed heat to space via longwave radiation (proportional to $4\sigma \bar{T}_A^3$). Additional longwave emission to space from the ocean surface and heat storage in the atmosphere result in corrections of order $1-\epsilon$ and δ, respectively.

This is the coupled mode described by Schopf (1983), who showed that the ocean cools on a *coupled* time scale τ_A that depends upon the ability of the atmosphere to radiate longwave to space. This time scale is substantially longer than the relaxation time scale of an *uncoupled* ocean: a few years versus a few months in the latter case. For an uncoupled ocean, the atmosphere is fixed and the ocean cools according to the surface turbulent flux and longwave emission from the ocean surface into the atmosphere (corresponding to a time scale slightly faster than τ_K). Coupled adjustment is slower because atmospheric longwave emission to space is inefficient compared to surface heat transfer by the turbulent flux (c.f. eq. 4). We show in the next section that if the atmosphere is perturbed by the forcing, the ocean adjustment is delayed as a result of the coupling.

In the coupled mode, the ocean temperature anomaly decays over the time scale λ_c^{-1} according to (5), where the tendency reflects the imbalance between heat transfer to the atmosphere through radiation and turbulent exchange. In contrast, the imbalance in the atmospheric budget (6) is nearly zero compared to the individual surface fluxes. (More precisely, the imbalance is equal to $\delta \frac{\partial T_A}{\partial t}$, which is of order δ.) As the ocean temperature evolves as a result of the forcing, the atmospheric temperature adjusts to maintain quasi-equilibrium with the ocean, so that the net transfer of heat to the atmosphere is nearly zero:

$$\delta\frac{\partial T_A}{\partial t} = \delta(-\lambda_c T_A) = O(\delta) = \frac{1}{\tau_K}(T_O - T_A) + \frac{\epsilon}{\tau_O}T_O - \frac{2}{\tau_A}T_A, \tag{10}$$

so that

$$T_A = \left(\frac{1+\epsilon\frac{\tau_K}{\tau_O}}{1+2\frac{\tau_K}{\tau_A}}\right)T_O + O(\delta\frac{\tau_K}{\tau_A}). \tag{11}$$

According to (10), the atmosphere, with its heat capacity that is small compared to that of the ocean, stays in equilibrium with the ocean as T_O changes. In the coupled mode, the ocean and atmospheric temperature anomalies are of the same order of magnitude. We define their ratio as α_c such that:

$$\alpha_c \equiv \frac{T_O}{T_A} = \frac{1+2\frac{\tau_K}{\tau_A}}{1+\epsilon\frac{\tau_K}{\tau_O}} + O(\delta\frac{\tau_K}{\tau_A}) \approx \frac{1+2\frac{\tau_K}{\tau_A}}{1+\epsilon\frac{\tau_K}{\tau_O}}. \tag{12}$$

b. The Atmospheric (or 'Fast') Mode

The other root of (7) represents a comparatively short time scale:

$$\lambda_a^{-1} \approx \frac{\delta\tau_K}{1+2\frac{\tau_K}{\tau_A}} = \frac{\frac{P_s}{g}C_{p,a}}{k+2\epsilon 4\sigma\bar{T}_A^3} \tag{13}$$

This time scale corresponds to adjustment of an atmospheric temperature anomaly, depending upon the atmospheric heat capacity $\frac{P_s}{g}C_{p,a}$ and the efficiency of heat loss both to space (equal to $4\epsilon\sigma\bar{T}_A^3$) and into the ocean (equal to $k + 4\epsilon\sigma\bar{T}_A^3$). Because of the physical interpretation of λ_a^{-1}, we refer to this mode as the 'atmospheric' mode.

The ratio of the two eigenvalues is

$$\frac{\lambda_c}{\lambda_a} = O(\delta\frac{\tau_K}{\tau_A}) \tag{14}$$

That is, the adjustment time λ_a^{-1} of the atmospheric mode is short and of order $\delta\frac{\tau_K}{\tau_A}$ compared to the coupled time scale λ_c^{-1}.

For this eigenmode, the atmospheric and ocean temperature anomalies are related by:

$$\frac{\partial T_O}{\partial t} = -\lambda_a T_O = \frac{1}{\tau_K}(T_A - T_O) + \frac{1}{\tau_A}T_A - \frac{1}{\tau_O}T_O, \tag{15}$$

so that:

$$
\begin{aligned}
T_O &= \left(\frac{1+\frac{\tau_K}{\tau_O}}{1+\frac{\tau_K}{\tau_A}} - \delta^{-1} \frac{1+\frac{2\tau_K}{\tau_A}}{1+\frac{\tau_K}{\tau_A}} \right)^{-1} T_A \\
&\equiv \alpha_a T_A \approx -\delta \left(\frac{1+\frac{\tau_K}{\tau_A}}{1+\frac{2\tau_K}{\tau_A}} \right) T_A
\end{aligned} \tag{16}
$$

For this mode, the atmospheric anomaly is greater than the ocean anomaly by order δ^{-1} and opposite in sign. Using (13) and (16), one can show that to order δ the dominant balances of the coupled system are:

$$
\begin{aligned}
\frac{\partial T_O}{\partial t} &\approx \left(\frac{1}{\tau_K} + \frac{1}{\tau_A} \right) T_A \\
\frac{\partial T_A}{\partial t} &\approx -\delta^{-1} \left(\frac{1}{\tau_K} + \frac{2}{\tau_A} \right) T_A,
\end{aligned} \tag{17}
$$

where the neglected terms are $O(\delta)$ compared to those retained. For the atmospheric mode, an atmospheric temperature anomaly is rapidly dissipated through transfer of energy to the ocean and space. According to (17), perturbations to T_A make the predominant contribution to the net surface heat exchange (and the tendencies of T_A and T_O), compared to the effect of the ocean temperature anomaly. The ocean response is $O(\delta)$ smaller than T_A due to the ocean's greater heat capacity and thermal inertia, so that the ocean makes a negligible contribution to the net surface heat flux under the atmospheric mode.

4. Response To Forcing

Dust plumes are observed to extend over the ocean as a succession of aerosol clouds corresponding to individual dust storms and a temporary increase in aerosol radiative forcing (e.g. Chiapello et al. 1999). Nonetheless, we began with the case of forcing that is constant in time, as a guide to understanding the response to more realistic forcing.

a. *Sudden Onset of Steady Forcing*

We calculate the response to steady forcing that begins abruptly:

$$F_T = \begin{cases} 0 & t < 0 \\ F_{T,0} & t \geq 0 \end{cases}$$

$$F_S = \begin{cases} 0 & t < 0 \\ F_{S,0} & t \geq 0 \end{cases} \tag{18}$$

The atmospheric and ocean temperature anomalies are assumed to be zero initially so that:

$$T_A = T_O = 0 \text{ at } t = 0. \tag{19}$$

1) Equilibrium Response to Steady Forcing

In response to steady forcing, the atmosphere and ocean come into a new equilibrium, denoted by $T_{A,E}$ and $T_{O,E}$ respectively, that can be derived by setting the time derivatives of (5) and (6) to zero. Then,

$$T_{A,E} = \frac{\left(1 + \frac{\tau_K}{\tau_O}\right) \tilde{F}_{T,0} + (\epsilon - 1)\frac{\tau_K}{\tau_O}\tilde{F}_{S,0}}{\frac{1}{\tau_A} + \frac{1-\epsilon}{\tau_O} + (2-\epsilon)\frac{\tau_K}{\tau_A \tau_O}} \tag{20}$$

and

$$T_{O,E} = \frac{\left(1 + \frac{\tau_K}{\tau_A}\right) \tilde{F}_{T,0} + \frac{\tau_K}{\tau_A}\tilde{F}_{S,0}}{\frac{1}{\tau_A} + \frac{1-\epsilon}{\tau_O} + (2-\epsilon)\frac{\tau_K}{\tau_A \tau_O}}, \tag{21}$$

where $\tilde{F}_{T,0} \equiv \frac{F_{T,0}}{\rho h C_{p,o}}$ and $\tilde{F}_{S,0} \equiv \frac{F_{S,0}}{\rho h C_{p,o}}$.

Regions of deep convection within the Tropics are typically humid throughout the depth of the troposphere (Sun and Oort 1995). As a result, longwave radiation from the surface is largely absorbed within the column, and most outgoing longwave to space originates within the upper troposphere. Even during dust outbreaks, when the aerosols are perched within the low humidity of the Saharan Air Layer (SAL) above the Trade Inversion (Prospero and Carlson 1970; Carlson and Prospero 1972), there can be substantial longwave absorption in the moist boundary layer underneath. Where there is large tropospheric absorption of surface longwave, ϵ is near unity, so that the atmospheric temperature perturbation needed to balance the forcing is approximately:

$$T_{A,E} \approx \tilde{F}_{T,0}\tau_A = \frac{F_{T,0}}{\epsilon 4\sigma \bar{T}_A^3} \tag{22}$$

For an atmosphere that is opaque to longwave radiation from the surface, all OLR originates within the atmosphere. In this limit ($\epsilon \to 1$), the atmospheric temperature adjusts to balance the forcing at TOA, and is entirely controlled by the forcing at this level (Pierrehumbert 1995). The climate sensitivity is the ratio of the surface temperature perturbation to the forcing, and according to (22) is approximated by τ_A, the time scale of longwave emission to space by the atmosphere. Due to the simplicity of our model, there are no amplifying feedbacks due to water vapor, the lapse-rate or clouds, for example.

The sea-air temperature difference is:

$$T_{O,E} - T_{A,E} = \frac{\left(1 - \frac{\tau_A}{\tau_O}\right)\tau_K \tilde{F}_{T,0} + \left[1 + (1-\epsilon)\frac{\tau_A}{\tau_O}\right]\tau_K \tilde{F}_{S,0}}{1 + (1-\epsilon)\frac{\tau_A}{\tau_O} + (2-\epsilon)\frac{\tau_K}{\tau_O}}. \tag{23}$$

For ϵ near unity and $\epsilon\bar{T}_A^3 \approx \bar{T}_O^3$ (so that $\tau_A \approx \tau_O$), this can be written approximately as:

$$F_{S,0} \approx (k + 4\sigma\bar{T}_O^3)(T_{O,E} - T_{A,E}) \tag{24}$$

That is, the surface forcing is balanced by adjusting the sea-air temperature difference.

The equilibrium temperature response is shown in Figure 2 for a range of forcing at TOA and at the surface. For an opaque atmosphere with ϵ equal to unity, the atmospheric temperature anomaly varies only with F_T, according to (22), and even for smaller values of ϵ remains only a weak function of the surface forcing. In contrast, the sea-air temperature difference is a stronger function of F_S as the net surface heat flux adjusts to balance the aerosol forcing at the surface. Figure 2 also shows that the ocean temperature anomaly $T_{O,E}$ depends mainly upon the TOA forcing, even though the ocean is forced directly only at the surface. This dependence of $T_{O,E}$ upon F_T is because the ocean is coupled to the atmosphere through the surface heat flux. One practical consequence is that estimates of ocean temperature trends forced by observed aerosol variations need to account for aerosol forcing at both the surface and TOA.

As the atmosphere becomes increasingly transparent to longwave radiation, the ocean replaces the atmosphere as the predominant longwave emitter, radiating directly to space to balance the TOA forcing. In the limit of vanishing ϵ, the ocean temperature is controlled entirely by the forcing at TOA: $T_{O,E} = \tau_O \tilde{F}_T$. In this limit, the atmospheric temperature remains a weak function of the surface forcing, and adjusts itself so that the anomalous surface heat flux balances the aerosol radiative divergence within the atmosphere: $\left(\frac{T_{A,E}-T_{O,E}}{\tau_K}\right) = \tilde{F}_T - \tilde{F}_S$.

In our model, the compensation of the surface forcing through adjustment of the sea-air temperature difference results from our approximation that the turbulent fluxes can be written as proportional to this difference. While this is a common parameterization of the turbulent flux of sensible heat, representation of the evaporative or latent heat flux is more complicated, and TOA forcing can be important to evaporation, which has implications for how aerosol forcing affects the hydrological cycle (Xian 2008).

2) Time-dependent Response to Steady Forcing

To satisfy the initial condition that the atmosphere and ocean temperature anomalies are originally zero, we need to combine the solution to the forced problem (in this case the equilibrium solution) with the two unforced modes, so that the total solution is:

$$\begin{aligned} T_A &= C_a \exp(-\lambda_a t) + C_c \exp(-\lambda_c t) + T_{A,E} \\ T_O &= C_a \alpha_a \exp(-\lambda_a t) + C_c \alpha_c \exp(-\lambda_c t) + T_{O,E} \end{aligned} \tag{25}$$

where α_a and α_c are the ratio of T_O to T_A for each of the unforced eigenmodes, and given approximately by (12) and (16). The coefficients C_a and C_c are chosen so that $T_A = T_O \equiv 0$

at the onset of the forcing at $t = 0$. Thus, (25) becomes:

$$\begin{aligned} 0 &= C_a + C_c + T_{A,E} \\ 0 &= \alpha_a C_a + \alpha_c C_c + T_{O,E} \end{aligned} \tag{26}$$

It can be shown that for small δ, the atmospheric mode (whose initial amplitude is given by C_a) is excited in proportion to $F_{T,0} - F_{S,0}$, the aerosol radiative divergence within the atmosphere. Likewise, the initial coupled model amplitude C_c is proportional to $F_{T,0}$ for $\tau_K \ll \tau_A$.

Figure 3 shows the response as a function of time for $F_{T,0} = -5\,\mathrm{Wm}^{-2}$ and $F_{S,0} = -10\,\mathrm{Wm}^{-2}$. These are typical climatological values of radiative forcing over the eastern subtropical Atlantic during NH summer, according to one model estimate (Miller et al. 2004). Aerosol models as a group compute a wide range of dust concentration, so that the forcing is correspondingly uncertain (Zender et al. 2004; Huneeus et al. 2011). Moreover, our model is highly simplified, lacking the ability to transfer energy beyond the spatial extent of the dust cloud, along with various feedbacks including those due to changes in water vapor, the atmospheric lapse-rate, and clouds. For these reasons, the magnitude of our adjusted temperature response is unlikely to closely match the anomaly derived from observations or even a more realistic model. Consequently, the few examples of forcing we present are intended to be merely illustrative of the model behavior. (Because of the model's linear dependence upon forcing, other solutions could be derived as linear combinations of the examples below.) What we believe is robust is the primary importance of TOA forcing during most of our model's adjustment to forcing, which we will show to be relatively insensitive to the neglected model feedbacks and magnitude of the aerosol forcing.

The atmospheric and ocean response are shown in red and blue, respectively in Figure 3. The bold line shows the total response. The dashed and dotted lines show the contributions to the total response by the coupled and atmospheric modes, respectively. Both unforced modes are important only initially because they decay with time. As a result, the total response approaches the equilibrium solution (denoted by a thin solid line). The top panel shows the response during the first month when the atmospheric mode is rapidly decaying. Coincident with this decay is a rapid but modest warming of the atmosphere as the column temperature comes into balance with the heating $F_T - F_S$. This warming reduces the sea-air temperature difference and the net loss of heat from the ocean to the atmosphere, offsetting the surface forcing F_S. Together the ocean and atmosphere cool over the time scale of the coupled mode (Figure 3b), until the adjusted temperature is in equilibrium with the forcing.

The evolution of the energy budgets during the adjustment to the forcing is shown in Figure 4. The anomalous surface energy budget is shown in blue, with each anomalous flux expressed in $\mathrm{K\,day^{-1}}$ and evaluated according to (5). Coincident with the rapid warming of the atmosphere during the first week, the anomalous turbulent flux of heat into the mixed layer (dashed) increases rapidly (Figure 4a). In equivalent terms, the loss of heat from the ocean to the atmosphere (i.e. including the unperturbed component) is reduced, offsetting the surface forcing (thin solid line). As a result, the ocean temperature no longer tracks the surface forcing, but eventually comes into balance with the TOA forcing. Over the longer interannual time scale corresponding to λ_c^{-1} (Figure 4b), the ocean cools, and both the turbulent and net longwave (dotted) fluxes oppose the surface forcing until the residual is zero (thick solid line) and equilibrium is reached.

The atmospheric heat budget is denoted in red, with its fluxes evaluated using (6). The turbulent flux anomaly (dashed) is equal and opposite to the corresponding turbulent flux in the mixed layer budget (5). As the atmosphere warms initially, the import of heat from the ocean to the atmosphere drops, almost completely compensating the aerosol heating (thin solid line, Figure 4a). Note that the atmospheric warming is tiny, and potentially difficult to observe, but causes a significant offset of the surface forcing due to the sensitivity of the turbulent flux to small changes in the sea-air temperature difference. Subsequent to the initial warming, the residual or net flux imbalance (equal to $\delta\frac{\partial T_A}{\partial t}$ and denoted by a thick solid line) becomes slightly negative so that the atmosphere cools together with the ocean over the longer coupled time scale (Figure 4b).

The total column ocean-atmosphere budget is shown in black, where the net imbalance (thick solid) is the difference between the outgoing longwave radiation (OLR, dotted) and the TOA forcing (thin solid). Initially, OLR increases as the atmosphere warms (Figure 4a), augmenting the TOA forcing, but on the longer coupled time scale, the atmosphere cools and OLR drops to oppose the forcing and restore balance (Figure 4b).

In summary, the atmosphere with its small heat capacity warms rapidly in response to the aerosol heating. This reduces the net loss of heat by the ocean to the atmosphere, which offsets the surface forcing. The atmosphere and ocean cool together over the coupled time scale until the reduction of OLR at the top of the atmosphere balances the TOA forcing.

The initial rapid compensation of nearly half of the surface forcing by the turbulent flux depends upon the initial warming of the atmosphere. Almost immediately, the ocean temperature tendency is far less than would result from the surface forcing alone. This compensation cannot be mimicked by a linear relaxation of the ocean temperature for two reasons. First, the ocean temperature would relax toward a value that depends only upon the surface forcing, inconsistent with Figure 2. Second, this relaxation would emerge over a slower time scale in proportion to the depth of the mixed-layer. Ocean models without an interactive atmosphere overestimate the initial response to surface forcing. The rapid atmospheric warming is due to aerosol heating. Only if this heating is small (as in the case of non-absorbing aerosols such as volcanic or tropospheric sulfates) can the atmospheric warming and initial offset of the surface forcing by the turbulent flux be neglected. This is shown in Figures 5 and 6 where the surface and TOA forcing are both -10 $\mathrm{W\,m^{-2}}$ so that the atmospheric radiative divergence due to the aerosols is zero. The initial atmospheric warming is small, and the turbulent and longwave fluxes adjust to the surface forcing solely over the longer coupled time scale. The amplitude of the atmospheric mode (C_a) is negligible because $F_{T,0} - F_{S,0}$ is zero. While the equilibrium response of the atmosphere and ocean is ultimately dominated by the TOA forcing, both T_A and T_O respond initially to the forcing at the surface and decouple from $F_{S,0}$ over the coupled time scale. Note also that the equilibrium response is twice as large as in Figure 3 even though the surface forcing is the same, consistent with the TOA forcing that is two times larger, consistent with (22).

The primary importance of forcing at TOA to the equilibrium response is illustrated by Figures 7 and 8, where forcing at the surface is specified to be strongly negative at -15 $\mathrm{W\,m^{-2}}$, but the TOA value is positive at 5 $\mathrm{W\,m^{-2}}$. This forcing might correspond to strongly absorbing aerosols like black carbon, although the absorption is probably excessive for dust particles. Despite the large reduction in radiation impinging upon the surface, the ocean cools negligibly in the first week (Figures 7a) before warming and exhibiting a positive temperature anomaly at equilibrium that is much larger in magnitude than the initial cooling. The ocean warms in spite of the negative surface forcing, because there is a large transfer of heat from the atmosphere to the ocean through the turbulent flux that ultimately results from the warming atmosphere (Figure 8a).

b. Single Impulse Forcing (δ-function)

Dust outbreaks and the associated radiative forcing over the tropical Atlantic result from intermittent wind erosion over upwind deserts. These discrete pulses of dust eventually merge downwind as a result of lateral mixing that creates a spatially continuous aerosol haze. However, near the African coast, the dust concentration increases intermittently with the passage of dusty air, and the associated radiative forcing can temporarily become several times higher than its background value.

Here, we compute the response to an isolated outbreak, where the time-dependence of the forcing is idealized as a delta-function:

$$\begin{aligned} F_T &= f_{T,0}\,\delta(t), \\ F_S &= f_{S,0}\,\delta(t) \end{aligned} \tag{27}$$

Expressing the forcing time-dependence as a delta-function assumes that the outbreak is limited to a duration that is short compared to the time scales of the response. This is certainly true in comparison to the interannual coupled time scale. It is less valid for the more rapid atmospheric time scale, but our results will be shown to be insensitive to this idealization. We use lower case to denote the forcing parameters $f_{T,0}$ and $f_{S,0}$, which represent a forcing impulse and have units of an energy impinging on a unit area, to distinguish them from the case of steady forcing in the previous subsection where the forcing parameters $F_{T,0}$ and $F_{S,0}$ have units of energy per unit area per unit time.

Because the forcing is zero after the impulse at $t = 0$, the general solution at subsequent times is a combination of the two unforced solutions:

$$\begin{aligned} T_A &= C_a \exp(-\lambda_a t) + C_c \exp(-\lambda_c t), \\ T_O &= C_a \alpha_a \exp(-\lambda_a t) + C_c \alpha_c \exp(-\lambda_c t) \end{aligned} \tag{28}$$

The coefficients C_a and C_c depend upon the forcing at $t = 0$. To solve for them, we integrate equations (5) and (6) for the temperature of the mixed-layer and atmosphere over the duration of the forcing:

$$\begin{aligned} \frac{P_s}{g} C_{p,a}[T_A(0+) - T_A(0-)] &= f_{T,0} - f_{S,0}, \\ \rho h C_{p,o}[T_O(0+) - T_O(0-)] &= f_{S,0}. \end{aligned} \tag{29}$$

where $0-$ refers to the instant just before the arrival of the dust cloud, and $0+$ refers to the moment immediately afterward, when the skies have cleared. If the ocean and atmospheric temperature are initially unperturbed, then $T_O(0-)$ and $T_A(0-)$ are zero, so that:

$$\begin{aligned} C_a + C_c &= \frac{g}{P_s C_{p,a}}(f_{T,0} - f_{S,0}), \\ \alpha_a C_a + \alpha_c C_c &= \frac{f_{S,0}}{\rho h C_{p,o}}, \end{aligned} \tag{30}$$

which can be solved for C_a and C_c:

$$\begin{aligned} C_c &= \frac{1}{\rho h C_{p,o}(\alpha_a - \alpha_c)} \left[\frac{\alpha_a}{\delta}(f_{T,0} - f_{S,0}) - f_{S,0} \right], \\ C_a &= \frac{1}{\rho h C_{p,o}(\alpha_a - \alpha_c)} \left[-\frac{\alpha_c}{\delta}(f_{T,0} - f_{S,0}) + f_{S,0} \right], \end{aligned} \tag{31}$$

Note that according to (12) and (16), respectively, $\alpha_c \sim O(1)$ while $\alpha_c \sim O(\delta)$. As in the case of steady forcing (Section 4.a.2), the initial amplitudes of the atmospheric and coupled modes can be shown to be proportional to $f_{T,0} - f_{S,0}$ and $f_{T,0}$, respectively for small δ. This means that beyond the initial few days following the onset of the forcing, after the atmospheric mode has decayed, forcing at TOA dominates the temperature response of both the ocean and atmosphere.

The temperature response following a dust outbreak is shown in Figure 9. The forcing is applied only for a single instant, but the amplitude is equivalent to forcings of $f_{T,0} = -5\,\mathrm{Wm}^{-2}$ and $f_{S,0} = -10\,\mathrm{Wm}^{-2}$ averaged over one week. That is, a succession of isolated outbreaks occurring once per week would correspond to a time-averaged forcing of $f_{T,0} = -5\,\mathrm{Wm}^{-2}$ and $f_{S,0} = -10\,\mathrm{Wm}^{-2}$. The atmospheric response is shown in red, with the total response as a thick solid line, and the contributions of the atmospheric and coupled modes as dotted and dashed lines, respectively. The ocean response is depicted similarly but in blue.

Following the outbreak, the atmosphere immediately warms, while the ocean cools (Figure 9a). However, the warming of the atmosphere is short-lived. After a few days (the time scale of the damped atmospheric mode), the atmosphere cools below its original temperature, and tracks the ocean cooling. Over the longer coupled time scale, both the ocean and atmospheric temperature anomalies decay toward their original values prior to the outbreak (Figure 9b).

The energy budgets for the ocean, atmosphere and column are shown in Figure 10. After the outbreak (idealized here to occur instantaneously), the aerosol forcing is zero, and the ocean temperature tendency is determined entirely by the imbalance in the net surface flux. Heat transfer from the ocean to the atmosphere that occured prior to the outbreak is reduced (indicated by the blue dashed line representing a positive turbulent flux anomaly into the ocean), causing a rapid cooling of the initial atmospheric temperature anomaly and an increase in ocean temperature. After a few days, the net surface flux has been restored to near its unperturbed value, and the tendency in both the ocean and atmospheric temperature anomalies is virtually indistinguishable from zero. Both temperatures asymptote back toward their unperturbed values but at a greatly reduced rate compared to the first few days after the outbreak.

c. Intermittent Forcing By a Series of Instantaneous Dust Outbreaks

We can use the response to a single dust outbreak to construct the response to a series of outbreaks. In general, the response to a single pulse of forcing at time t' is:

$$\begin{aligned} T_A(t,t') &= C_a \exp[-\lambda_a(t-t')] + C_c \exp[-\lambda_c(t-t')], \\ T_O(t,t') &= C_a\alpha_a \exp[-\lambda_a(t-t')] + C_c\alpha_c \exp[-\lambda_c(t-t')], \end{aligned} \tag{32}$$

where C_a and C_c are given by the solution to (30). If the forcing consists of dust outbreaks at regular intervals Δ starting at time $t = 0$, so that after the N+1$^{\text{st}}$ pulse at time $t = N\Delta$, the forcing is:

$$\begin{aligned} F_T &= \sum_{n=0}^{N} f_{T,n}\delta(t-n\Delta); \\ F_S &= \sum_{n=0}^{N} f_{S,n}\delta(t-n\Delta) \end{aligned} \tag{33}$$

then the response is:

$$\begin{aligned} T_A(t) &= \sum_{n=0}^{N} C_{a,n} \exp[-\lambda_a(t-n\Delta)] + \sum_{n=0}^{N} C_{c,n} \exp[-\lambda_c(t-n\Delta)], \\ T_O(t) &= \sum_{n=0}^{N} C_{a,n}\alpha_a \exp[-\lambda_a(t-n\Delta)] + \sum_{n=0}^{N} C_{c,n}\alpha_c \exp[-\lambda_c(t-n\Delta)]. \end{aligned} \tag{34}$$

where the coefficients $C_{a,n}$ and $C_{c,n}$ are related to the forcing parameters through $f_{T,n}$ and $f_{S,n}$ based upon equations analogous to (30).

For simplicity, consider a series of identical outbreaks so that $f_{T,n} = f_{T,0}$ and $f_{S,n} = f_{S,0}$ and the coefficients $C_{a,n}$ and $C_{c,n}$ are independent of n. Then, we can write T_A as:

$$T_A(t) = C_a \exp(-\lambda_a t) \sum_{n=0}^{N} \exp(\lambda_a n\Delta) + C_c \exp(-\lambda_c t) \sum_{n=0}^{N} \exp(\lambda_c n\Delta) \tag{35}$$

We use the identity $\sum_{n=0}^{N} x^n = \frac{x^{N+1}-1}{x-1}$ and define $G(a, N) \equiv \frac{e^a - e^{-aN}}{e^a - 1}$ to write:

$$T_A(t) \;=\; C_a \exp(-\lambda_a t_d) G(\lambda_a \Delta, N) + C_c \exp(-\lambda_c t_d) G(\lambda_c \Delta, N) \qquad (36)$$

where t_d is the time since the most recent dust outbreak, so that $t_d = t - N\Delta$. Consider, for example, the last term on the right-hand side of (36) representing the accumulated effect of the coupled modes excited by successive outbreaks. The factor $\exp(-\lambda_c t_d)$ is related to the attenuation of the coupled mode since the most recent outbreak at $T = N\Delta$. This attenuation is nearly zero because the time since the most recent outbreak is negligible compared to the mode's adjustment time scale λ_c^{-1}.

The atmospheric response T_A to successive dust outbreaks given by (36) can be compared to the response following a single dust event (28). For the coupled mode, the effect of superposition is given by the term $G(\lambda_c \Delta, N)$, which is plotted in Figure 11. Here, $N\Delta$ is the number of days separating the first and most recent dust outbreaks, and the horizontal axis (corresponding to $\lambda \Delta N$) is the number of modal time scales that have elapsed since the first outbreak. (Figure 11 is constructed by using $\lambda = \lambda_c$ from the coupled mode.) Each dot represents a single outbreak. The term G is unity for $N = 0$ and for small N, G increases linearly as the number of outbreaks increases. Successive outbreaks reinforce each other, adding to the response. However, for $\Delta N \geq \lambda_c^{-1}$ (that is, for times longer than the coupled mode adjustment time), the response eventually saturates, asymptoting toward an upper bound of $(\lambda_c \Delta)^{-1}$. (Note that $(\lambda_c \Delta)^{-1} \gg 1$.) The response to additional outbreaks is canceled by the evanescence of the original outbreaks that are decaying as λ_c^{-1}. One practical implication is that the response to a few dusty years (corresponding to the coupled time scale) is as large as the response to a longer-lasting dusty period.

Reinforcement of the temperature response by repeated excitation of the atmospheric mode (the first term on the right side of eq. 36) is much smaller. This is because the time scale of the atmospheric mode is on the order of a few days. This is comparable to the spacing between observed outbreaks, so that the response forced by one outbreak has nearly vanished by the time the next outbreak occurs. Almost all of the growth of the response is due to reinforcement by successive excitations of the coupled mode.

Figure 12 shows the response to a succession of weekly dust outbreaks (so that $\Delta = 7$ days). Each outbreak occurs only for a brief instant, but the time-averaged forcing is identical to the steady forcing case illustrated in Figure 3, where $F_T = -5\,\mathrm{Wm}^{-2}$ and $F_S = -10\,\mathrm{Wm}^{-2}$. The response grows gradually over the coupled mode time scale due to superposition of the response to successive outbreaks. The ultimate cooling is identical to that of the steady forcing case, reflecting the identical time-averaged forcing. Note that the ocean cools more steadily than the atmosphere, which shows a temporary warming after each outbreak. This is due to the higher thermal inertia of the ocean mixed-layer (reflected by the factor of δ in α_a in eq. 16). While the overall cooling of the ocean and atmosphere is due to superposition of the coupled mode excited by successive outbreaks, the atmospheric mode causes a temporary warming of the atmosphere and a cooling of the ocean that rapidly decays.

During NH summer, dust outbreaks are often organized by African waves (e.g. Karyampudi and Carlson 1988), so that successive outbreaks occur every few days, a period shorter than the 7 days interval used to calculate Figure 12. On the face of it, Figure 11 might suggest that more frequent events (whose recurrence interval Δ is shorter) would lead to a larger eventual response (proportional to $(\lambda_c \Delta)^{-1}$). However, if we decrease the time between outbreaks while keeping the long-term average forcing the same, then the forcing per event ($f_{T,0}$ and $f_{S,0}$) should decrease in proportional to the interval Δ. Thus, for a given time-averaged forcing, the asymptotic temperature response (given by the product of $f_{T,0}$ and the asymptotic value of $G(\lambda\Delta, N)$) should be independent of the time between outbreaks. Moreover, the time required to reach equilibration should also be independent of the outbreak frequency, since according to the horizontal axis of Figure 11, this depends upon the time elapsed since the first outbreak (given by ΔN) compared to the coupled mode adjustment time λ_c^{-1}. For a given elapsed time, a greater outbreak frequency must be exactly offset by a greater number of outbreaks. In summary, for a given time-averaged forcing, the eventual maximum temperature response and time required to reach it are independent of Δ, the period between outbreaks.

d. *Succession of Dust Outbreaks With Gradual Onset*

Observed dust outbreaks over the eastern tropical Atlantic last for a day or two (Chiapello et al. 1999), and Figure 13 shows the response for a series of outbreaks where the forcing associated with each pulse varies in time according to

$$h(t-t',T) = \begin{cases} 0 & t<0 \\ \frac{t-t'}{T^2}\exp[-\frac{t-t'}{T}] & t\geq 0 \end{cases}. \tag{37}$$

For each outbreak, starting at $t = t'$, the forcing increases up to time T, and decays gradually thereafter. If the outbreaks start at $t = 0$, and occur at uniform interval Δ, then the forcing after $N + 1$ outbreaks is:

$$\begin{aligned} F_T &= \sum_{n=0}^{N} f_{T,n}\frac{t-n\Delta}{T^2}\exp\left[-\frac{t-n\Delta}{T}\right]; \\ F_S &= \sum_{n=0}^{N} f_{S,n}\frac{t-n\Delta}{T^2}\exp\left[-\frac{t-n\Delta}{T}\right]. \end{aligned} \tag{38}$$

To be consistent with the case of recurring but instantaneous outbreaks (Figure 13), $f_{T,n}$ and $f_{S,n}$ are chosen so that the time-averaged forcing is -5 $\mathrm{W m^{-2}}$ at TOA and -10 $\mathrm{W m^{-2}}$ at the surface. Figure 13 shows the response for $T = 1$ day and outbreaks separated by $\Delta = 7$ days. (The solution is calculated numerically, although we give an exact, analytic solution in Appendix B.) The response resembles that shown in Figure 12, demonstrating that the main features of the realistic response are captured by our idealized case with instantaneously applied forcing. Both cases show an overall cooling trend, consistent with the TOA forcing. The atmospheric response peaks about a day after the maximum in forcing associated with each outbreak. The effect of extending the forcing duration (while keeping the time-averaged forcing unchanged) is to moderate the excitation of the atmospheric mode that is manifest as rapid atmospheric warming and ocean cooling following each outbreak.

The dotted line in Figure 13 shows the ocean temperature calculated assuming that there is no surface energy exchange with the atmosphere. In this case, the ocean cools off far more rapidly. In contrast, the ocean temperature in the full model very quickly decouples from the surface forcing in order to come into balance with the TOA forcing, as described above.

5. Discussion of Model Approximations

a. Lateral redistribution of heat beyond the region of forcing

Our model assumes that the atmosphere responds to dust radiative forcing without exchanging energy beyond the region of forcing. However, the tropical atmosphere adjusts efficiently to localized forcing over a broad region due to its large Rossby radius of deformation compared to mid-latitudes (Yu and Neelin 1997). The tropic-wide response to El Niño is an example of heat redistribution that arises from an anomaly originally confined to the equatorial eastern Pacific (Klein et al. 1999; Sobel et al. 2002). Modeling studies show that the tropical atmosphere responds to aerosol radiative forcing by exchanging energy with regions outside of the aerosol cloud (Miller and Tegen 1999; Rodwell and Jung 2008).

Our model is intended to interpret the change of SST in the eastern tropical Atlantic, a dusty environment where tropical cyclones form. Lateral heat redistribution to the remainder of the Tropics and mid-latitudes is potentially important. This process can be introduced into the model heuristically as a linear restoring term $-\frac{1}{\tau_D}T_A$ in the heat budget of the atmosphere (6), where τ_D is the time scale for dynamical adjustment. Assuming as before that ϵ is near unity and that $\tau_K \ll \tau_A, \tau_O$, and also that $\tau_K \ll \tau_D$, we can write:

$$\lambda_c \approx \frac{1}{\tau_A} + \frac{1}{\tau_D}. \tag{39}$$

This could have been anticipated on physical grounds, because in the absence of dynamics, adjustment of OLR (proportional to $-\frac{1}{\tau_A}T_A$) is the only way for a coupled atmosphere-ocean column that is opaque in the longwave to balance any forcing. The addition of dynamical heat transport (also proportional to T_A in our simple formulation) augments the adjustment by OLR in (6). The coupled-mode time scale in the presence of dynamics is:

$$\lambda_c^{-1} \approx \frac{\tau_A \tau_D}{\tau_A + \tau_D}, \tag{40}$$

which can be compared to $\lambda_c^{-1} \approx \tau_A$ in (9), calculated in the absence of dynamics. In Appendix A, we estimate that $\tau_A = 332$ days. Following the development of an El Niño event in the Pacific, tropical temperature responds in other oceans with a lag ranging from three to six months (Klein et al. 1999; Sobel et al. 2002). The effect of this is to reduce the coupled-mode time scale to between roughly 70 to 120 days, compared to the value of 222 days calculated in Appendix A in the absence of dynamics. However, this time scale remains longer than that of the atmospheric mode, suggesting that during most of its adjustment, the temperature response is dominated by the coupled mode, whose amplitude is approximately proportional to the TOA forcing.

An additional effect of lateral mixing is to reduce the magnitude of the equilibrium perturbation to the atmospheric temperature. This can be seen by analogy to (22). A smaller temperature perturbation is needed to compensate the forcing if heat can be exchanged by both lateral transport and longwave emission, compared to the effect of the latter acting alone. Lateral transport reduces the equilibrium temperature, but not the initial warming associated with the atmospheric mode, whose reduction of the surface turbulent and longwave fluxes strongly offsets the surface aerosol forcing.

b. *Vertical mixing and coupling of boundary layer and free tropospheric temperature*

Deep convection drives the tropical lapse-rate toward a moist adiabat (Betts 1982; Xu and Emanuel 1989), but between convective events when dry and warm mid-tropospheric air subsides into the boundary-layer, an inversion typically forms (Augstein et al. 1974). Over the eastern tropical Atlantic, the inversion is reinforced by the arrival of the Saharan Air Layer (Carlson and Prospero 1972). Within the main development region of Atlantic tropical cyclones, the inversion is eventually disrupted by the return of deep convection, and during NH summer, the passage of the ascending phase of an African wave typically restores the moist adiabat every few days (Karyampudi and Carlson 1988). This causes tropical soundings to alternate between a near-moist adiabat and soundings with a strong inversion at the top of the boundary layer Dunion and Velden (2004); Dunion and Marron (2008); Dunion (2011).

That convection is inhibited by the arrival of the SAL (Wong and Dessler 2005), when dust radiative forcing is largest, requires closer examination of our model assumption that the troposphere is always well-mixed. Vertical mixing is central to our model behavior because air at the surface is rapidly warmed by heating of the aerosol layer. The warmed surface air transfers heat into the ocean through the turbulent and longwave fluxes, opposing the aerosol forcing at the surface, which is subsequently replaced in importance by the TOA forcing that controls the surface air temperature. Thus, opposition to the surface forcing depends upon the ability of the atmosphere to mix heat from the dust layer down to the surface.

To see the effect of the SAL on our model, we carry out a thought experiment and divide the troposphere into separate layers representing the boundary layer and free troposphere, respectively. We consider two limiting cases where the dust and the associated forcing during an outbreak are concentrated entirely within the boundary layer, or else in the free troposphere within the SAL. If the dust layer and forcing are confined to the boundary layer, the surface air would warm more rapidly compared to the atmospheric time scale of our original model (13), because the boundary layer has only a fraction of the mass of the entire tropospheric column. In this case, SST would decouple from the surface forcing more quickly than in our original model due to the more rapid warming of the boundary layer and surface air.

For the case of the aerosol heating confined to the SAL within the free troposphere, vertical mixing would be initially inhibited due to the strong inversion created by the aerosols.

This would delay warming of the surface, allowing the surface forcing to cool the ocean without opposition from the anomalous turbulent and longwave fluxes. Within a few days, the arrival of convection associated with the disturbed phase of an African wave would break down the inversion (Augstein et al. 1974), mixing heat from the free troposphere down to the surface. SST would decouple from the surface forcing in proportion to the strength of this mixing. For this case, the inhibition of deep convection by the SAL would extend the duration within which surface forcing was the predominant control upon SST.

Near the African coast, summertime dust concentration is highest in the free troposphere. However, the mass of dust falls off downwind over the Atlantic, due to setting of particles into the boundary layer, and eventually the ocean. Thus, dust and its radiative forcing are increasingly concentrated within the boundary layer as the aerosol crosses the Atlantic, and this would reduce the influence of the surface forcing upon SST, even if mixing across the inversion were completed inhibited.

The key uncertainty here is the rate at which heat is mixed down from the SAL within the free troposphere. Vertical mixing is difficult to parameterize within a simple model since it depends in a complicated way upon the dynamics of convection and the large-scale circulation, along with their interaction with dust radiative heating. This uncertainty suggests that models of the SST response to dust radiative forcing need to represent this process with fewer assumptions and with greater complexity than allowed by our simple model. However, if heat is mixed down on a time-scale that is short compared to the coupled time scale λ_c^{-1} (on the order of a few months), then the results of our original model should be largely unmodified, since the surface forcing has little time to cool the ocean, due the large inertia of the latter. In this case, temperature anomalies in the atmosphere and ocean will be controlled primarily by TOA forcing during most of their adjustment.

6. Conclusions

We have calculated how temperature adjusts to radiative forcing in a simple coupled ocean-atmosphere model. As previously noted (e.g. Cess et al. 1985), the atmospheric temperature in the new equilibrium is determined primarily by the forcing at TOA, and surface forcing has only a secondary influence (Figure 2). Our model shows additionally that TOA forcing has a primary influence not only upon the equilibrium value of atmospheric temperature, but during nearly the entire approach to equilibrium. This is because the transient atmospheric mode decays rapidly (within a few days), leaving only the coupled mode that is excited approximately in proportion to the TOA forcing. Forcing at TOA is also a strong constraint upon the ocean temperature as well, as a result of heat transfer through the surface turbulent and net longwave fluxes.

The primacy of TOA forcing to the ocean temperature results even though only forcing at the surface is present in the mixed-layer energy budget (5). Surface forcing is rapidly replaced in importance by TOA forcing within a few days after the forcing onset, after the atmosphere has adjusted to aerosol forcing. This adjustment perturbs the exchange of heat between the ocean and atmosphere, which opposes the surface forcing. This exchange is particularly important for absorbing aerosols that warm the atmosphere while reducing the net radiative flux into the surface. Despite a strong reduction of radiation into the ocean surface, SST rises in response to positive TOA forcing (Figure 7). This is because the atmosphere must warm so that the forcing can be balanced by OLR, and this warming causes heating of the ocean through the turbulent and longwave surface fluxes.

In some studies, the influence of the atmosphere and surface heat flux upon SST are represented as a relaxation process proportional to the ocean temperature anomaly T_O, with relaxation on a time scale proportional to the mixed layer heat capacity. Our results suggest two problems with this representation. First, the ocean temperature adjusts only to the surface forcing (since the TOA forcing is omitted from the model in the absence of a budget for the atmosphere). This is in contradiction to the primary dependence of SST upon forcing at TOA in Figure 2. Second, our model shows that the anomalous surface flux becomes important on a time scale related to the atmospheric heat capacity that is rapid compared to any realistic relaxation time constructed from the much larger mixed-layer heat capacity. In technical terms, the contribution kT_A makes the largest initial contribution to the turbulent flux $k(T_A - T_O)$ and this contribution is omitted when the flux is represented solely in terms of the ocean temperature anomaly. Models of ocean temperature that omit the response of the atmosphere to the aerosol forcing will overestimate the influence of forcing at the surface. Beyond a few days following the onset of aerosol forcing (a duration determined by the time scale of the atmospheric mode), both the sign and magnitude of the temperature response by the ocean and atmosphere are determined primarily by the forcing at TOA. Only within a few days of forcing onset does the surface forcing solely influence the ocean temperature. Even within this initial period, the tendency of SST remains small due to the large mixed-layer heat capacity.

One practical implication of our model is that any calculation of the ocean temperature change by observed trends in dust aerosols needs to account for the TOA forcing and the atmospheric response. Only if the atmospheric temperature anomaly is small (corresponding to small atmospheric radiative divergence by the forcing, for example by non-absorbing aerosols) is the negative feedback by the net surface heat flux negligible. For the example of the SST trend forced by industrial sulfates or volcanic aerosols, the omission of the TOA forcing might be justified quantitatively. However, this doesn't change the primary contribution of the TOA forcing to the ocean response. In this example, the TOA and surface values are identical so that the primacy of the TOA forcing is obscured.

Our coupled model is limited by certain approximations. For example, the model cannot respond to aerosol radiative forcing by redistributing energy beyond the forcing region; forcing at TOA can be balanced only by adjusting OLR. For an atmosphere that is nearly opaque to longwave radiation, this tightly couples the TOA forcing to atmospheric temperature. If lateral redistribution of energy is represented as a relaxation process, then this transport augments the OLR anomaly and shortens the adjustment time. Nonetheless, for a nearly opaque atmosphere, TOA forcing continues to control both the atmospheric and ocean temperatures over most of their approach to equilibrium.

We also assume that the atmosphere moves energy instantaneously between the surface and the upper troposphere where most of the longwave radiation to space occurs. Our assumption is most valid in convecting regions (where tropical cyclones are observed to develop), as departures from a moist adiabatic lapse-rate are small (Betts 1982; Xu and Emanuel 1989). However, observations show that dust aerosols within the SAL suppress convection and vertical mixing (Dunion and Velden 2004; Wong and Dessler 2005). The replacement of the surface forcing with the TOA value in determining the evolution of the forced temperature anomaly depends upon heating of the surface air by aerosols, and thus vertical mixing of energy between the aerosol layer and the surface. It is difficult to represent this mixing in our simple model, and we identify this process as a key uncertainty. The rapid feedback displayed by our simple model, where the net surface heat flux between the atmosphere and ocean opposes and rapidly reduces the influence of the surface forcing depends upon this mixing being fast compared to the coupled mode time scale. This does not seem like a restrictive assumption in the Atlantic Main Development Region for tropical cyclones, where the column is mixed by deep convection every few days, but our model behavior should be tested with a more realistic model.

Our model lacks feedbacks by atmospheric water vapor and the vertical lapse-rate, both of which combine to amplify the effect of an initial forcing, according to more comprehensive models (Soden and Held 2006). These processes not only increase the magnitude of the temperature response in our model, but also lengthen the adjustment time scales of the unforced modes (Hansen et al. 1985). Because of the limitations of our simple model, we have not emphasized the magnitude of the temperature response to dust aerosol forcing (which itself is uncertain). We are currently using a general circulation model to calculate the temperature response to dust which avoids some of the more restrictive approximations in our model. Nonetheless, we believe that the primary importance of TOA forcing throughout most of the temperature adjustment is robust, since this result depends on the disparate adjustment time scales of the atmospheric and coupled modes.

Our results indicate that the influence of dust aerosols upon tropical cyclones through changes in SST should be tested with a model that is more comprehensive than an energy budget for the ocean mixed-layer, where surface fluxes are independent of the atmospheric state. The use of an atmospheric general circulation model to test the effect of dust upon SST would have the additional benefit of allowing a broader range of interactions between dust and tropical cyclones, possibly suggesting additional hypotheses to account for their observed anticorrelation. Dust may inhibit tropical cyclones through other mechanisms that we have not addressed here.

Acknowledgments.

I am grateful for the thoughtful comments of two anonymous reviewers and Amato Evan (who suggested representing dynamical transport as linear relaxation). I also benefited from discussions with Peter Knippertz, Natalie Mahowald, Carlos Pérez, Adam Sobel and Charlie Zender. Thanks also to Lilly Del Valle for drafting Fig. 1. This work was supported by the Climate Dynamics Program of the National Science Foundation under ATM-06-20066.

APPENDIX A

Numerical Values

We specify the thermal inertia of the atmosphere using $C_{p,a} = 1004\,\mathrm{J\,kg^{-1}\,K^{-1}}$, tropospheric depth $P_s = 800\,\mathrm{hPa}$, and $g = 9.81\,\mathrm{m\,s^{-2}}$. The ocean thermal inertia is computed assuming that the mixed-layer has a heat capacity of $C_{p,o} = 4000\,\mathrm{J\,kg^{-1}\,K^{-1}}$, density $\rho = 10^3\,\mathrm{kg\,m^{-3}}$, and depth $h = 20\,\mathrm{m}$. The mixed-layer depth is chosen to be characteristic of shallow values found during NH summer in the eastern tropical Atlantic, a location of tropical cyclone development during this season. Larger mixed layers would lengthen the coupled time scale and slow the adjustment. For our chosen values, the ratio of the atmospheric to ocean thermal inertia $\delta = \frac{P_s}{\rho g h}\frac{C_{p,a}}{C_{p,o}} = 0.10$ and decreases as the mixed-layer deepens toward the Caribbean to the west.

To calculate the longwave relaxation time scales τ_O and τ_A for the ocean and atmosphere, respectively, we specify unperturbed temperatures of $\bar{T}_O = 300\,\mathrm{K}$ and $\bar{T}_A = 260\,\mathrm{K}$. Furthermore, we assume that the longwave broadband opacity ϵ equals 0.7 so that most radiation comes from the atmosphere rather than the ocean surface. Then, $\tau_O = \frac{\rho h C_{p,o}}{4\sigma \bar{T}_O^3} = 151\,\mathrm{days}$ and $\tau_A = \frac{\rho h C_{p,o}}{\epsilon 4\sigma \bar{T}_A^3} = 332\,\mathrm{days}$.

To derive τ_K, the relaxation time scale for the anomalous turbulent flux, which is the sum of the anomalous fluxes of sensible and latent heat $S + LE$, we use the common parameterizations:

$$\hat{S} = C_{p,a}\rho_a C_D |u_s| (\hat{T}_O - \hat{T}_{A,S})$$
$$L\hat{E} = L\rho_a C_D |u_s| [\hat{q}_A - q^*(\hat{T}_O)]. \qquad \text{(A1)}$$

Here the 'hat' symbol (ˆ) indicates the total value of a variable, including both its unperturbed and anomalous components, so that $\hat{T}_O = \bar{T}_O + T_O$, for example. In (A1), ρ_a

is the density of air at the surface, equal to $1.3\,\mathrm{kg\,m^{-3}}$, $C_D = 10^{-3}$ is a bulk coefficient, $u_s = 7\,\mathrm{m\,s^{-1}}$ is a typical value of the surface wind speed, $\hat{T}_{A,S}$ is the surface air temperature, $L = 2.5 \times 10^5\,\mathrm{J\,kg^{-1}}$ is the latent heat of vaporization, $\hat{q}_A$ is the surface air specific humidity and q^* is the saturation specific humidity evaluated at the sea surface temperature $\hat{T}_O$. We can linearize both of these formulas assuming that the surface air temperature anomaly $T_{A,S}$ is equal to the anomalous atmospheric temperature T_A. Then:

$$
\begin{aligned}
S &= C_{p,a}\rho_a C_D |u_s| (T_O - T_A) \\
LE &= L\rho_a C_D |u_s| [r\frac{dq^*}{dT}(T_O - T_A) + (1-r)T_A]
\end{aligned}
\tag{A2}
$$

where r is the surface relative humidity (expressed as a fraction), and $\frac{dq^*}{dT}$ is evaluated at the unperturbed surface air temperature, taken as $\bar{T}_{A,S} = 298\,\mathrm{K}$. We assume that the surface relative humidity is large (i.e. near unity) and neglect the last term in the parameterization of latent heat, although Xian (2008) shows that this can be important in some circumstances. Then, we can write the total turbulent heat flux as:

$$
LE + S = C_{p,a}\rho_a C_D |u_s| \left(1 + \frac{L}{C_{p,a}}\frac{dq^*}{dT}\right)(T_O - T_A) \equiv k(T_O - T_A) \tag{A3}
$$

so that the turbulent efficiency $k = 37\,\mathrm{W\,m^{-2}\,K^{-1}}$ and $\tau_K = 25$ days. Note that while each of τ_A, τ_O, and τ_K increase with the mixed-layer depth h, the ratio of the time scales (and the comparative restoring efficiency of radiation and turbulent heat transfer) are independent of this depth.

These numerical values are used in the calculations shown in the figures, and correspond to relaxation times of the coupled and atmospheric modes equal to $\lambda_c^{-1} = 222$ days and $\lambda_a^{-1} = 2$ days, respectively.

We have chosen $\epsilon = 0.7$ to represent an atmosphere that is partly transparent in the longwave (allowing some radiation emitted by the surface to escape to space), but with most outgoing longwave emitted by the atmosphere. To facilitate physical interpretation of the equations, we occasionally set the longwave opacity ϵ equal to one to simplify the algebra. Our model is highly idealized, but its behavior described in this article depends mainly upon the fact that δ is small. That is, the ocean mixed-layer has much greater thermal inertia than the atmosphere.

The input parameters and derived constants are summarized in Table 1.

APPENDIX B

Solution For Gradually Applied Forcing

To derive the evolution of the coupled atmosphere and ocean in response to forcing with arbitrary time-dependence, we write (5) and (6) in matrix form:

$$\frac{\partial}{\partial t}\mathbf{T} = \mathbf{AT} + \mathbf{f} \tag{B1}$$

where:

$$\mathbf{T} = \begin{pmatrix} T_A \\ T_O \end{pmatrix}, \tag{B2}$$

$$\mathbf{A} = \begin{pmatrix} -\left(\frac{1}{\tau_K} - \frac{2}{\tau_A}\right)\frac{1}{\delta} & \left(\frac{1}{\tau_K} + \frac{\epsilon}{\tau_O}\right)\frac{1}{\delta} \\ \frac{1}{\tau_K} + \frac{1}{\tau_A} & -\frac{1}{\tau_K} - \frac{1}{\tau_O} \end{pmatrix},$$

and

$$\mathbf{f} = \begin{pmatrix} \frac{1}{\delta}\frac{F_T - F_S}{\rho h C_{p,o}} \\ \frac{F_S}{\rho h C_{p,o}} \end{pmatrix}. \tag{B3}$$

In Section 3, we found the unforced modes that correspond to the eigenvalues and eigenvectors of $\mathbf{A}$. That is:

$$\mathbf{AE} = \mathbf{E\Lambda} \text{ or } \mathbf{A} = \mathbf{E\Lambda E^{-1}} \tag{B4}$$

where

$$\mathbf{\Lambda} = \begin{pmatrix} -\lambda_c & 0 \\ 0 & -\lambda_a \end{pmatrix}, \tag{B5}$$

is a diagonal matrix containing the eigenvalues of $\mathbf{A}$, given approximately by (9) and (13), and the matrix $\mathbf{E}$

$$\mathbf{E} = \begin{pmatrix} 1 & 1 \\ \alpha_c & \alpha_a \end{pmatrix}, \tag{B6}$$

contains the eigenvectors that are linearly independent.

Then we can write the general solution $\mathbf{T}$ in terms of the eigenvectors:

$$\mathbf{T} = \mathbf{E}\mathbf{X}, \tag{B7}$$

so that $\mathbf{X}$ satisfies

$$\frac{\partial}{\partial t}\mathbf{X} = \mathbf{\Lambda}\mathbf{X} + \mathbf{E^{-1}f} \tag{B8}$$

The advantage of (B8) over (B1) is that the former consists of uncoupled first-order equations that can be solved individually for the elements of $\mathbf{X}$. Given $\mathbf{X}$, we can invert (B7) to solve for the ocean and atmospheric temperature anomalies as they evolve in response to the forcing.

Consider a single episode of forcing that increases gradually starting at time t' over a duration T before decaying gradually, as given by (37):

$$\begin{aligned} F_T &= f_{T,0}\, h(t-t',T), \\ F_S &= f_{S,0}\, h(t-t',T). \end{aligned} \tag{B9}$$

Then, defining:

$$g(t,T,\lambda) \equiv \frac{1}{(1-\lambda T)^2}\left\{\exp(-\lambda t) - \left[1 + (1-\lambda T)\frac{t}{T}\right]\exp\left(-\frac{t}{T}\right)\right\}, \tag{B10}$$

we can write the solution for the evolution of the atmospheric and ocean temperature response as:

$$\begin{aligned} T_A &= C_c g(t-t',T,\lambda_c) + C_a g(t-t',T,\lambda_a) \\ T_O &= C_c\alpha_c g(t-t',T,\lambda_c) + C_a\alpha_a g(t-t',T,\lambda_a) \end{aligned} \tag{B11}$$

where C_c and C_a are given by (31).

Figure 14 shows the temperature response during the first ten days for different onset intervals T. Again, $f_{T,0}$ and $f_{S,0}$ are chosen so that the forcing equals -5 Wm^{-2} at TOA and -10 Wm^{-2} at the surface when averaged over the first week. For $T = 0$ days, the forcing is a single impulse applied instantaneously as in Section 4.2, and the solution is identical to that given in Figure 9. For forcing that increases gradually over one-half day ($T = 0.5$) and one day ($T = 1$), respectively, the atmospheric warming is increasingly muted. In contrast, the ocean cooling is less sensitive to the duration of the forcing increase, and within a week, both the atmosphere and ocean have cooled compared to their unperturbed values, which are slowly restored over the coupled time scale λ_c^{-1}. In summary, a gradual increase in forcing (compared to an instantaneous impulse) reduces the initial atmospheric warming and ocean cooling, but the response over the longer coupled time scale is essentially independent of how abruptly the forcing is applied.

For a series of outbreaks that increase over $T = 1$ day and are separated by a week, the solution (B11) equals that plotted in Figure 13.

REFERENCES

Augstein, E., H. Schmidt, and F. Ostapoff, 1974: The vertical structure of the atmospheric planetary boundary layer in undisturbed trade winds over the Atlantic ocean. *Boundary-Layer Meteorol.*, **6**, 129–150.

Betts, A. K., 1982: Saturation point analysis of moist convective overturning. *J. Atmos. Sci.*, **39**, 1484–1505.

Carlson, T. N. and J. M. Prospero, 1972: The large-scale movement of Saharan air outbreaks over the northern equatorial Atlantic. *J. Appl. Meterol.*, **11**, 283–297.

Cess, R. D., G. L. Potter, S. J. Ghan, and W. L. Gates, 1985: The climatic effects of large injections of atmospheric smoke and dust: A study of climate feedback mechanisms with one- and three-dimensional climate models. *J. Geophys. Res.*, **90**, 12 937–12 950.

Chiapello, I., J. M. Prospero, J. R. Herman, and N. C. Hsu, 1999: Detection of mineral dust over the North Atlantic Ocean and Africa with the Nimbus 7 TOMS. *J. Geophys. Res.*, **104 (D8)**, 9277–9291.

Chou, C., J. D. Neelin, U. Lohmann, and J. Feichter, 2005: Local and remote impacts of aerosol climate forcing on tropical precipitation. *J. Climate*, **18**, 4621–4636.

de Boyer Montegút, C., G. Madec, A. S. Fischer, A. Lazar, and D. Iudicone, 2004: Mixed layer depth over the global ocean: An examination of profile data and a profile-based climatology. *J. Geophys. Res.*, **109**, C12003, doi:10.1029/2004JC002378.

Dunion, J. P., 2011: Rewriting the climatology of the Tropical North Atlantic and Caribbean Sea atmosphere. *J. Climate*, **24**, 893–908, doi:10.1175/2010JCLI3496.1.

Dunion, J. P. and C. S. Marron, 2008: A reexamination of the Jordan mean tropical sounding based on awareness of the Saharan Air Layer: Results from 2002. *J. Climate*, **21**, 5242–5253.

Dunion, J. P. and C. S. Velden, 2004: The impact of the Saharan air layer on Atlantic tropical cyclone activity. *Bull. Amer. Meteorol. Soc.*, **March**, 353–365.

Evan, A. T., 2007: Comment on "how nature foiled the 2006 hurricane forecasts". *Eos, Trans. Am. Geophys. Union*, **88 (26)**, 271.

Evan, A. T., J. Dunion, J. A. Foley, A. K. Heidinger, and C. S. Velden, 2006: New evidence for a relationship between Atlantic tropical cyclone activity and African dust outbreaks. *Geophys. Res. Lett.*, **33**, L19813, doi:10.1029/2006GL026408.

Evan, A. T., D. J. Vimont, A. K. Heidinger, J. P. Kossin, and R. Bennartz, 2009: The Role of Aerosols in the Evolution of Tropical North Atlantic Ocean Temperature Anomalies. *Science*, **324 (5928)**, 778–781, doi:10.1126/science.1167404.

Evan, A. T., et al., 2008: Ocean temperature forcing by aerosols across the Atlantic tropical cyclone development region. *Geochem. Geophys. Geosyst.*, **9**, Q05V04, doi:10.1029/2007GC001774.

Foltz, G. R. and M. J. McPhaden, 2008a: Impact of Saharan dust on tropical North Atlantic SST. *J. Climate*, **21**, 5048–5060, doi:doi:10.1175/2008JCLI2232.1.

Foltz, G. R. and M. J. McPhaden, 2008b: Trends in Saharan dust and tropical Atlantic climate during 1980 – 2006. *Geophys. Res. Lett.*, **35**, L20706, doi:10.1029/2008GL035042.

Forster, P., et al., 2007: Changes in atmospheric constituents and in radiative forcing. *Climate Change 2007: The Physical Science Basis. Contribution of Working Group I to the Fourth Assessment Report of the Intergovernmental Panel on Climate Change*, S. Solomon, D. Qin, M. Manning, Z. Chen, M. Marquis, K. Averyt, M.Tignor, and H. Miller, Eds., Cambridge University Press, Cambridge, United Kingdom and New York, NY, USA, chap. 2.

Hansen, J., G. Russell, A. Lacis, I. Fung, D. Rind, and P. Stone, 1985: Climate response times: Dependence on climate sensitivity and ocean mixing. *Science*, **229**, 857–859, doi: 10.1126/science.229.4716.857.

Huneeus, N., et al., 2011: Global dust model intercomparison in AeroCom phase I. *Atmos. Chem. Phys.*, **11**, 7781–7816, doi:10.5194/acp-11-7781-2011.

Karyampudi, V. M. and T. N. Carlson, 1988: Analysis and numerical simulation of the Saharan Air Layer and its effect upon easterly wave disturbances. *J. Atmos. Sci.*, **45**, 3102–3136.

Klein, S. A., B. J. Soden, and N.-C. Lau, 1999: Remote sea surface temperature variations during ENSO: Evidence for a tropical atmospheric bridge. *J. Climate*, **12**, 917–932.

Lau, K. M. and J. M. Kim, 2007a: How nature foiled the 2006 hurricane forecasts. *Eos Trans. AGU*, **88**, 105–107.

Lau, K. M. and K. M. Kim, 2007b: Cooling of the Atlantic by Saharan dust. *Geophys. Res. Lett.*, **34**, L23811, doi:10.1029/2007GL031538.

Lau, K.-M. and K.-M. Kim, 2007c: Reply to comment on "how nature foiled the 2006 hurricane forecasts,". *Eos, Trans. Am. Geophys. Union*, **88**, 271.

Martińez Avellaneda, N., N. Serra, P. J. Minnett, and D. Stammer, 2010: Response of the eastern subtropical Atlantic SST to Saharan dust: A modeling and observational study. *J. Geophys. Res.*, **115**, C08015, doi:10.1029/2009JC005692.

Miller, R. L. and I. Tegen, 1998: Climate response to soil dust aerosols. *J. Climate*, **11**, 3247–3267.

Miller, R. L. and I. Tegen, 1999: Radiative forcing of a tropical direct circulation by soil dust aerosols. *J. Atmos. Sci.*, **56**, 2403–2433.

Miller, R. L., I. Tegen, and J. Perlwitz, 2004: Surface radiative forcing by soil dust aerosols and the hydrologic cycle. *J. Geophys. Res.*, **109**, D04203, doi:10.1029/2003JD004085.

Pierrehumbert, R. T., 1995: Thermostats, radiator fins, and the runaway greenhouse. *J. Atmos. Sci.*, **52**, 1784–1806.

Prospero, J. and T. Carlson, 1970: Radon-222 in the North Atlantic trade winds: Its relationship to dust transport from Africa. *Science*, **167**, 974–977.

Rodwell, M. J. and T. Jung, 2008: Understanding the local and global impacts of model physics changes: An aerosol example. *Q. J. R. Met. Soc.*, **134**, 1479–1497, doi:10.1002/qj.298.

Schollaert, S. and J. Merrill, 1998: Cooler sea surface west of the Sahara Desert correlated to dust events. *Geophys. Res. Lett.*, **25**, 3529–3532.

Schopf, P. S., 1983: On equatorial waves and El Niño. ii: effects of air-sea thermal coupling. *J. Phys. Oceanogr.*, **13**, 1878–1893.

Sobel, A. H., I. M. Held, and C. S. Bretherton, 2002: The ENSO signal in tropical tropospheric temperature. *J. Climate*, **15**, 2702–2706.

Soden, B. J. and I. M. Held, 2006: An assessment of climate feed- backs in coupled atmosphere-ocean models. *J. Climate*, **19**, 3354–3360.

Sun, D.-Z. and A. H. Oort, 1995: Humidity-temperature relationships in the tropical troposphere. *J. Climate*, **8**, 1974–1987.

Wong, S. and A. E. Dessler, 2005: Suppression of deep convection over the tropical North Atlantic by the Saharan Air Layer. *Geophys. Res. Lett.*, **32**, L09808, doi:10.1029/2004GL022295.

Xian, P., 2008: Seasonal migration of the ITCZ and implications for aerosol radiative impact. Ph.D. thesis, Columbia University.

Xu, K.-M. and K. A. Emanuel, 1989: Is the tropical atmosphere conditionally unstable. *Mon. Weather Rev.*, **117**, 1471–1479.

Yu, J. Y. and J. D. Neelin, 1997: Analytic approximations for moist convectively adjusted regions. *J. Atmos. Sci.*, **54**, 1054–1063.

Zender, C. S., R. L. Miller, and I. Tegen, 2004: Quantifying mineral dust mass budgets: Systematic terminology, constraints, and current estimates. *Eos, Trans. AGU*, **85 (48)**, 509,512.

List of Tables

Table 1. Input parameters and derived quantities.

Variable	*Symbol*	*Value*
Input parameters for atmos.		
Specific heat of air	$C_{p,a}$	1004 $\mathrm{J\,kg^{-1}\,K^{-1}}$
Tropospheric depth	P_s	800 hPa
Gravity	g	9.81 $\mathrm{m\,s^{-2}}$
Unperturbed tropos. T	$\bar{T}_A$	260 K
Unperturbed surf. air T	$\bar{T}_{A,S}$	298 K
Surf. density of air	ρ_a	1.3 $\mathrm{kg\,m^{-3}}$
Bulk coefficient	C_D	10^{-3}
Surf. wind speed	u_s	7 $\mathrm{m\,s^{-1}}$
Latent heat of vapor.	L	2.5×10^5 $\mathrm{J\,kg^{-1}}$
Turb. efficiency	k	37 $\mathrm{W\,m^{-2}\,K^{-1}}$
Tropos. LW emissivity	ϵ	0.7
Input parameters for ocean		
Specific heat of seawater	$C_{p,o}$	4000 $\mathrm{J\,kg^{-1}\,K^{-1}}$
Seawater density	ρ	10^3 $\mathrm{kg\,m^{-3}}$
Mixed-layer depth	h	20 m
Unperturbed ocean T	$\bar{T}_O$	300 K
Derived ratio of thermal inertia		
Ratio (atmos. to ocean)	δ	0.10
Derived adjustment time scales		
Ocean	τ_O	151 days
Tropos.	τ_A	332 days
Turb. flux	τ_K	25 days
Derived modal time scales		
Coupled mode	λ_c^{-1}	222 days
Atmos. mode	λ_a^{-1}	2 days

List of Figures

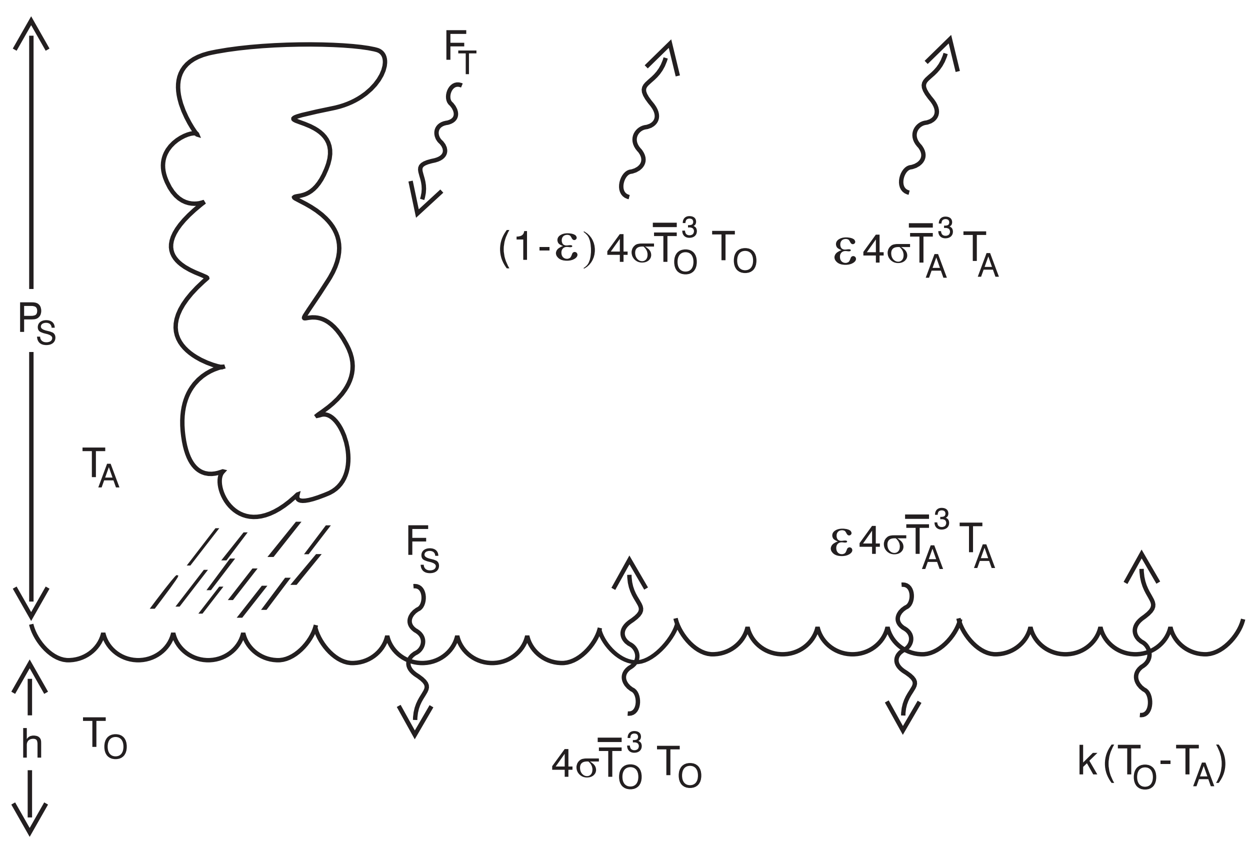

Fig. 1. Schematic of simple coupled model.

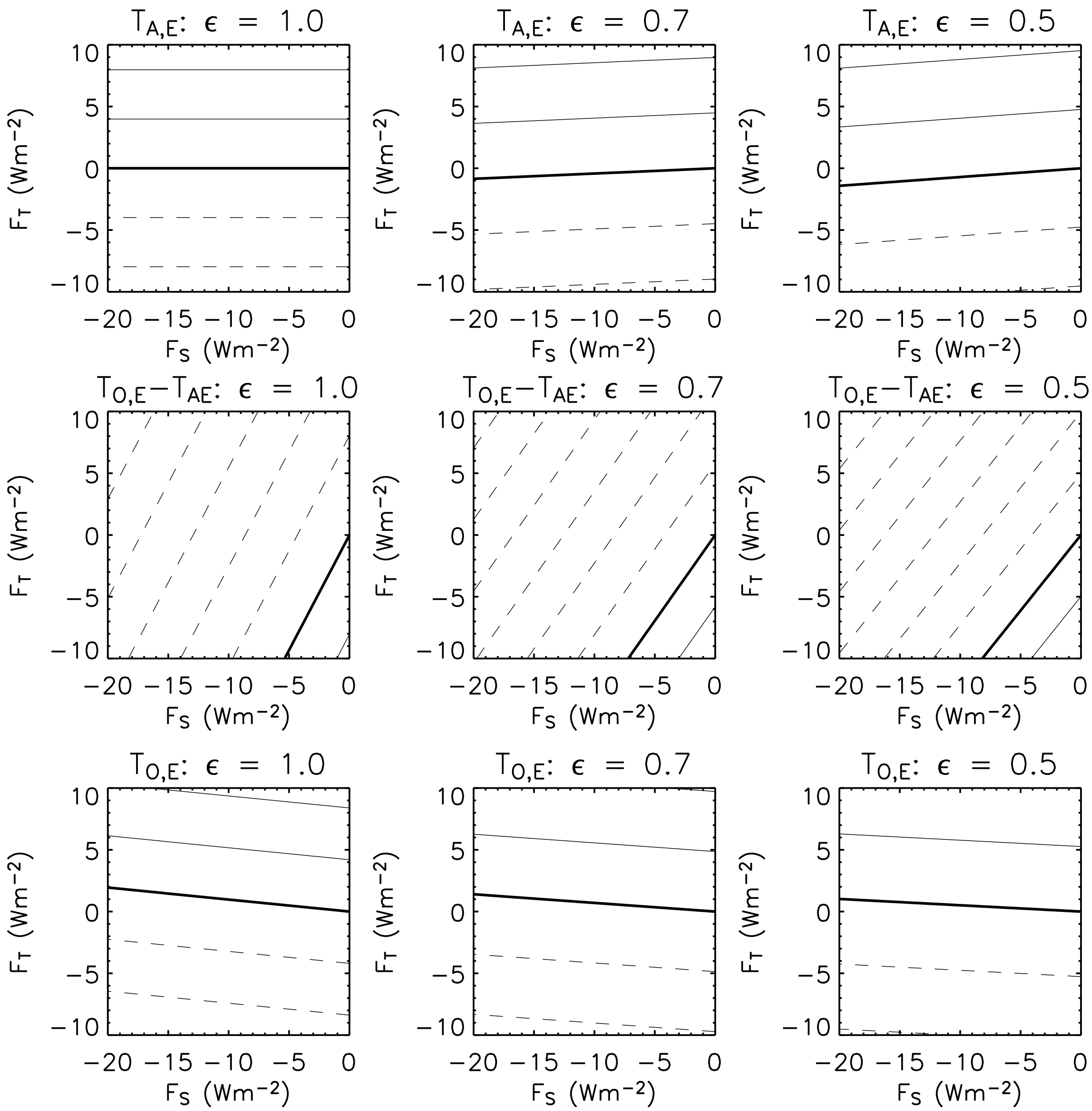

FIG. 2. Equilibrium response of anomalous air temperature $T_{A,E}$, ocean temperature $T_{O,E}$ (both with contour interval of 1 K) and the sea-air difference $T_{O,E} - T_{A,E}$ (contour interval of 0.1 K) as a function of forcing at TOA (F_T) and the surface (F_S). Positive contours are solid, and negative contours are dashed. The thick solid contour corresponds to zero.

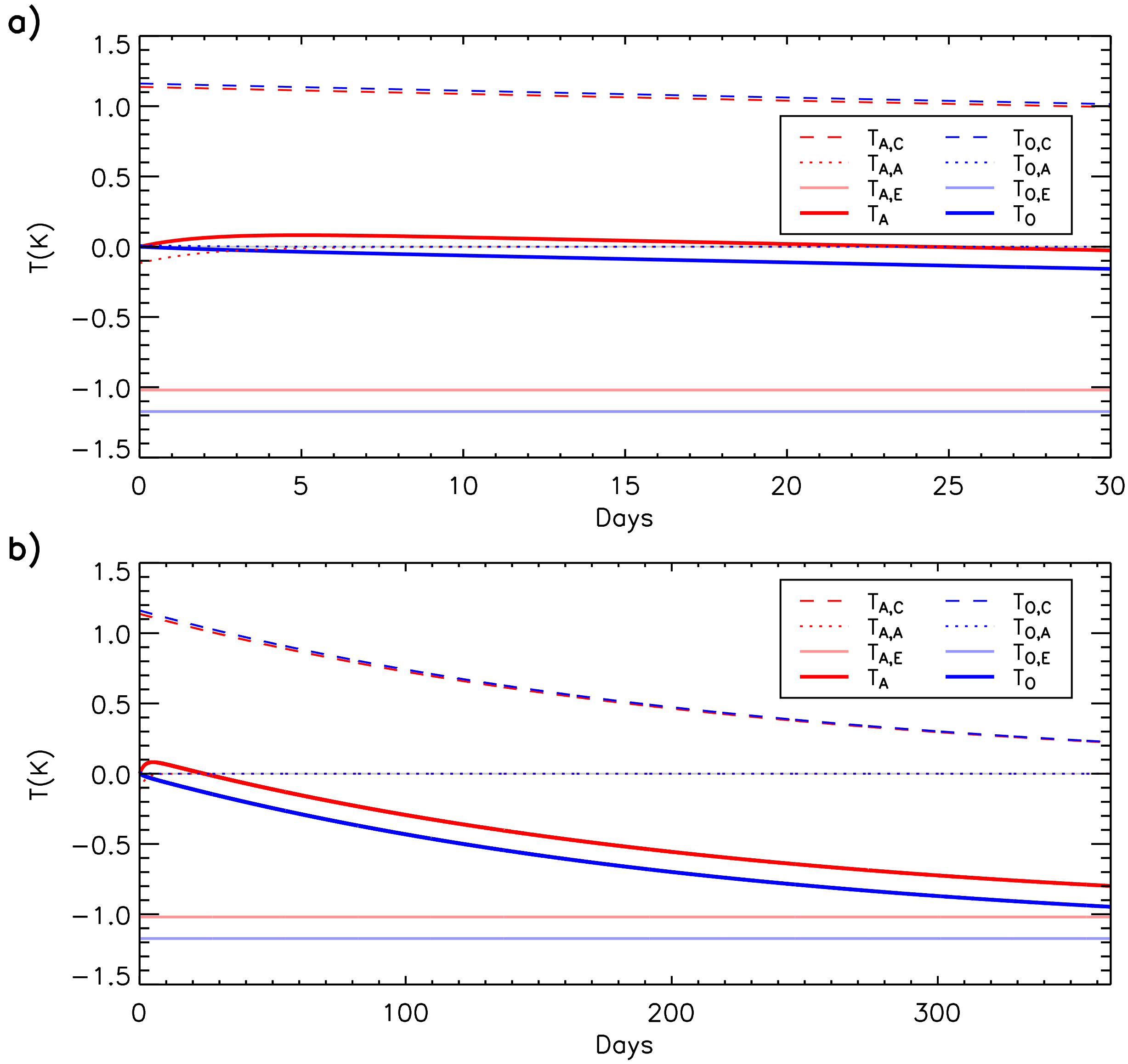

FIG. 3. Anomalous atmospheric (red) and ocean (blue) temperature during the first a) 30 days after the onset of forcing, and b) 365 days. The forcing is -5 Wm^{-2} at TOA and -10 Wm^{-2} at the surface. The total response is depicted by the heavy solid line. The equilibrium response is given by the thin solid line. The ephemeral contributions of the atmospheric and coupled modes, proportional to $C_a \exp(-\lambda_a t)$ and $C_c \exp(-\lambda_c t)$ respectively, are given by the dotted and dashed lines.

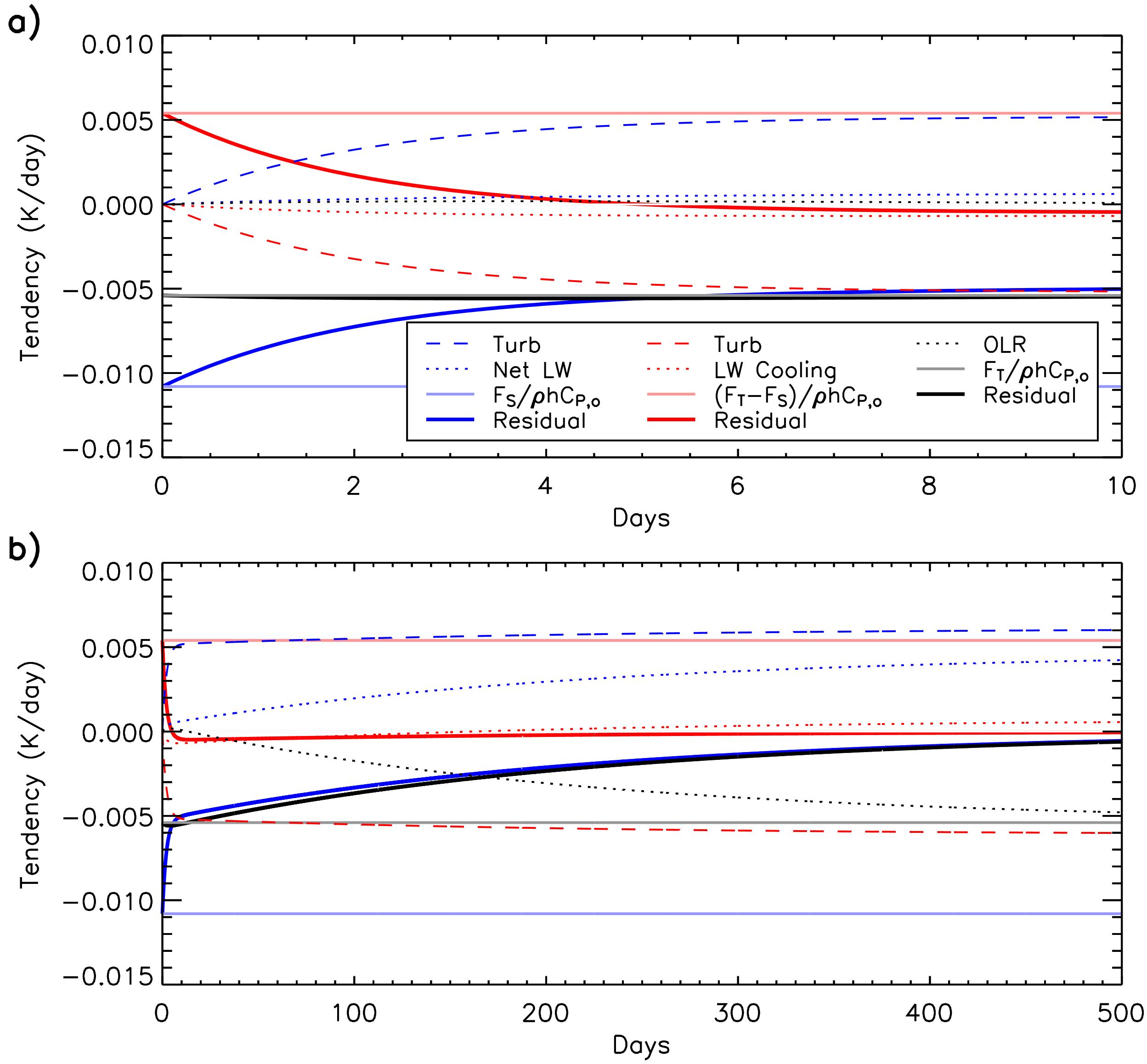

FIG. 4. Anomalous energy budgets during the first a) 10 days after the onset of forcing, and b) 500 days. The forcing is -5 $\mathrm{W m^{-2}}$ at TOA and -10 $\mathrm{W m^{-2}}$ at the surface. In blue are fluxes comprising the surface energy budget according to (5): turbulent heat transfer from the atmosphere to the ocean (dashed), net longwave radiation (dotted), the surface forcing (thin solid), and their residual (thick solid). In red are the contributions to the atmospheric energy budget: turbulent heat transfer from the ocean to the atmosphere (dashed), net longwave cooling (dotted), aerosol heating (thin solid), and their residual (thick solid). In black is the energy budget at the top of the atmosphere: outgoing longwave radiation (dotted), forcing at TOA (thin solid), and their residual (thick solid). All fluxes have units of $\mathrm{K\,day^{-1}}$.

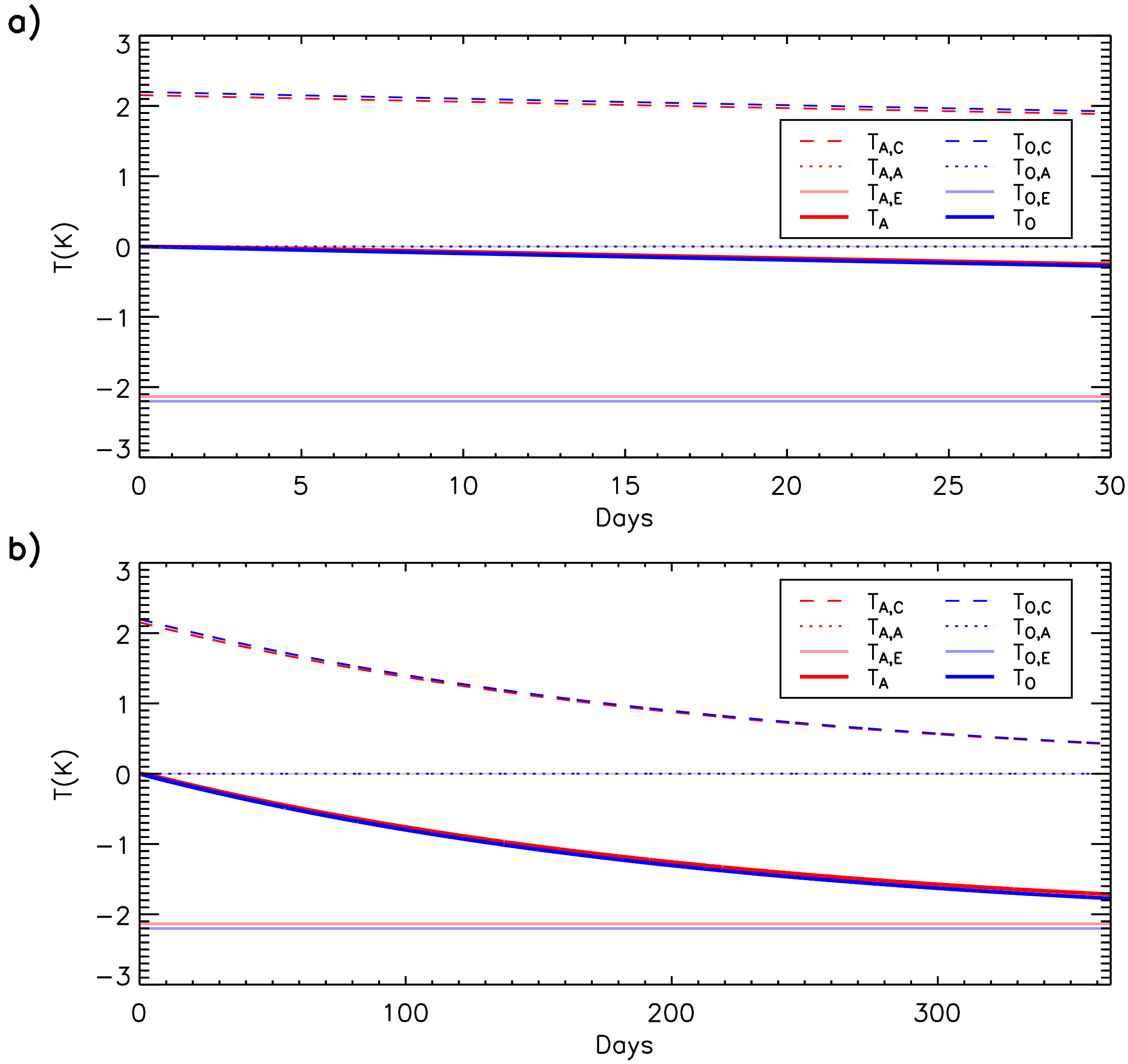

FIG. 5. Same as Figure 3, but with forcing of -10 Wm^{-2} at both TOA and the surface (so that the corresponding atmospheric radiative divergence is zero).

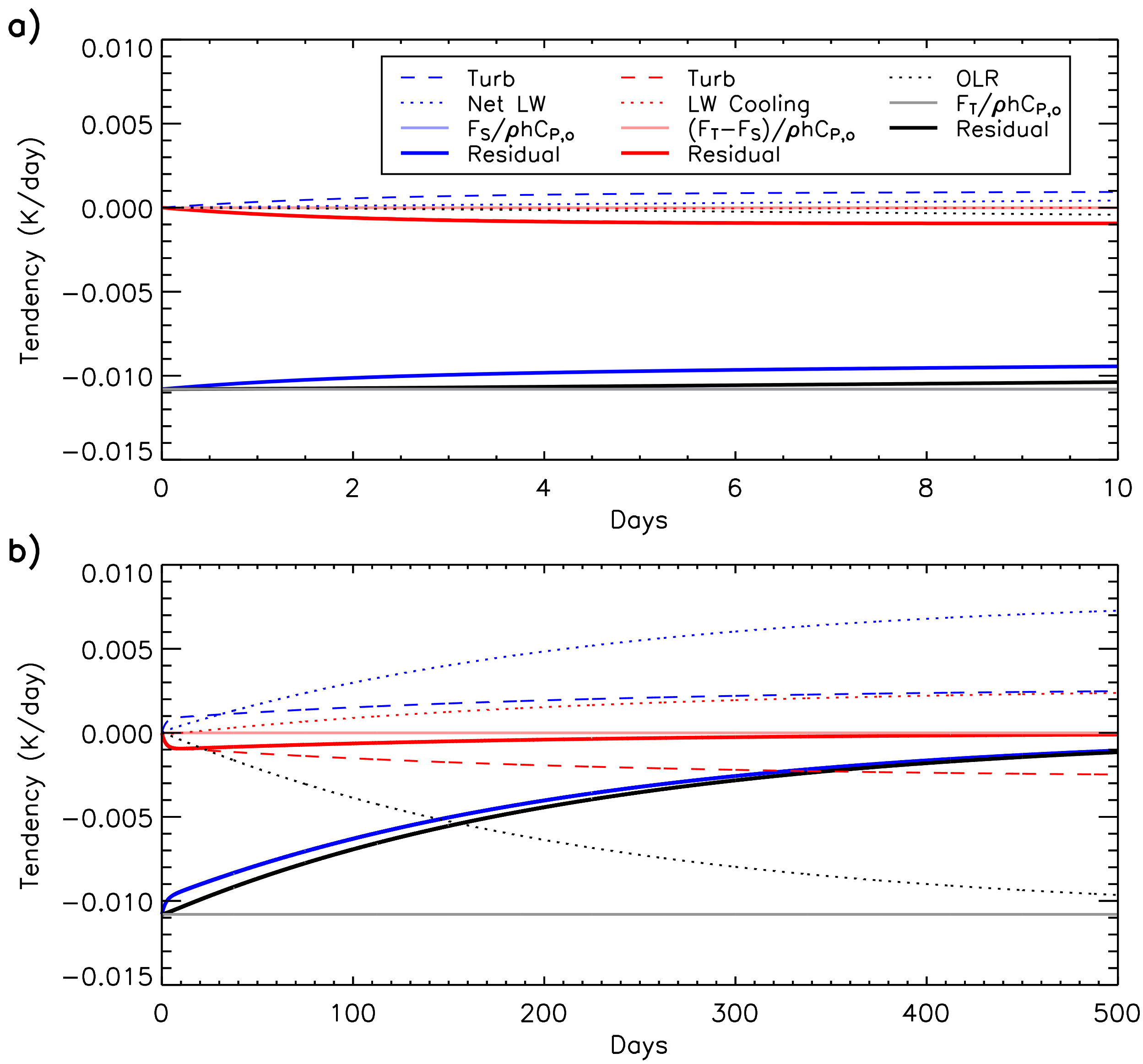

FIG. 6. Same as Figure 4, but with forcing of -10 Wm^{-2} at both TOA and the surface (so that the corresponding atmospheric radiative divergence is zero).

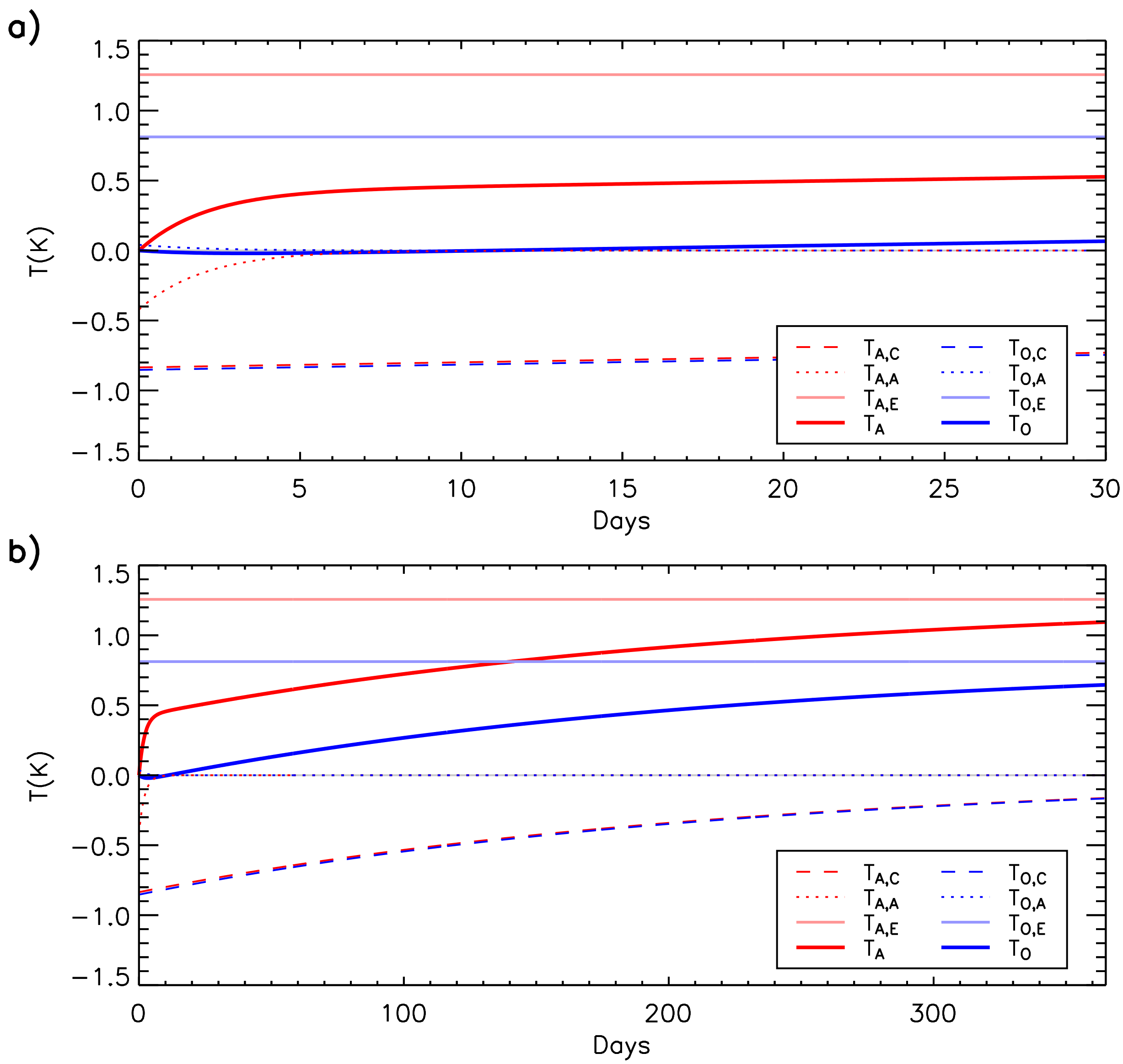

FIG. 7. Same as Figure 3, but with forcing of 5 $\mathrm{Wm^{-2}}$ at TOA and -15 $\mathrm{Wm^{-2}}$ at the surface.

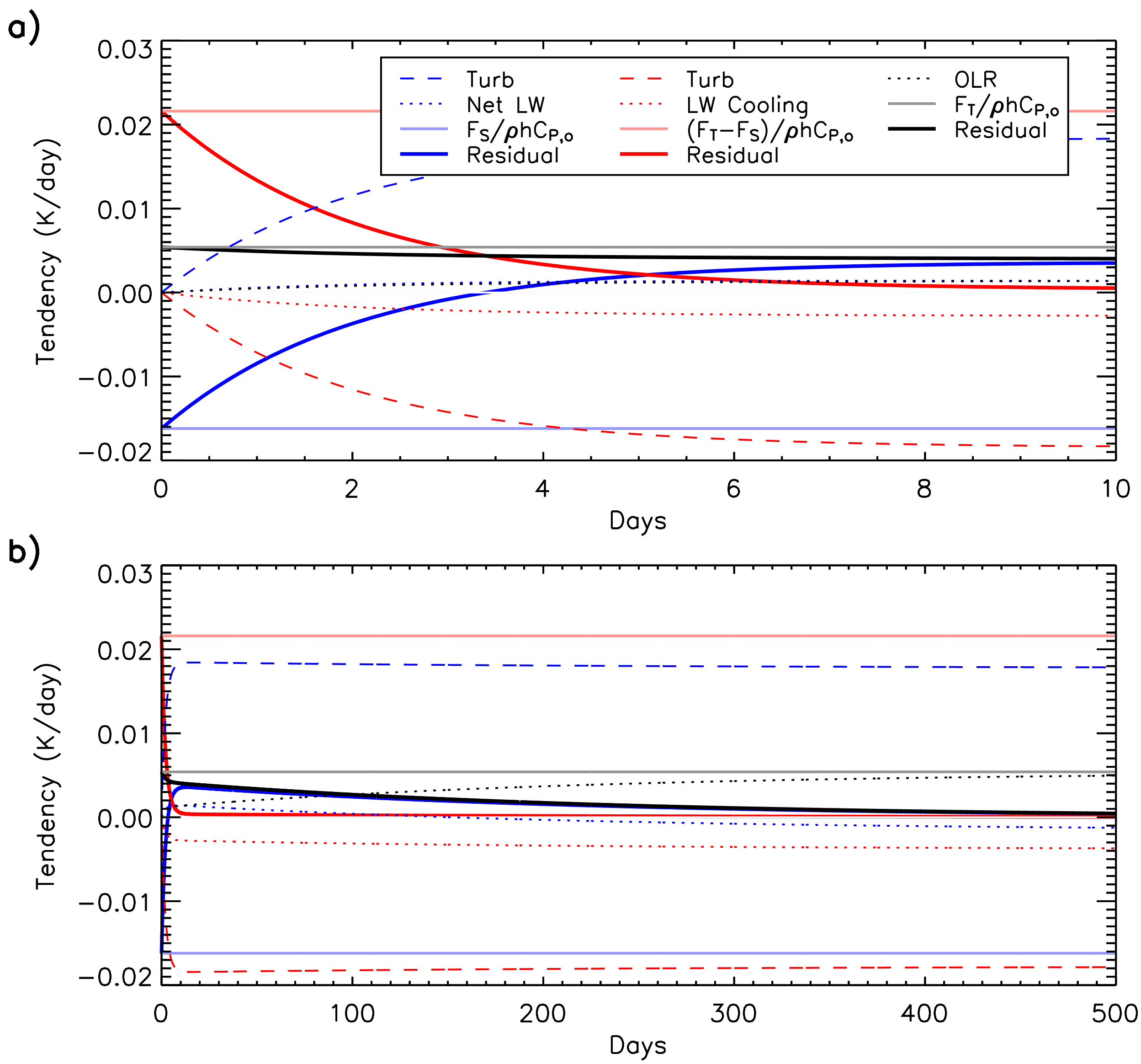

FIG. 8. Same as Figure 4, but with forcing of 5 Wm^{-2} at TOA and -15 Wm^{-2} at the surface.

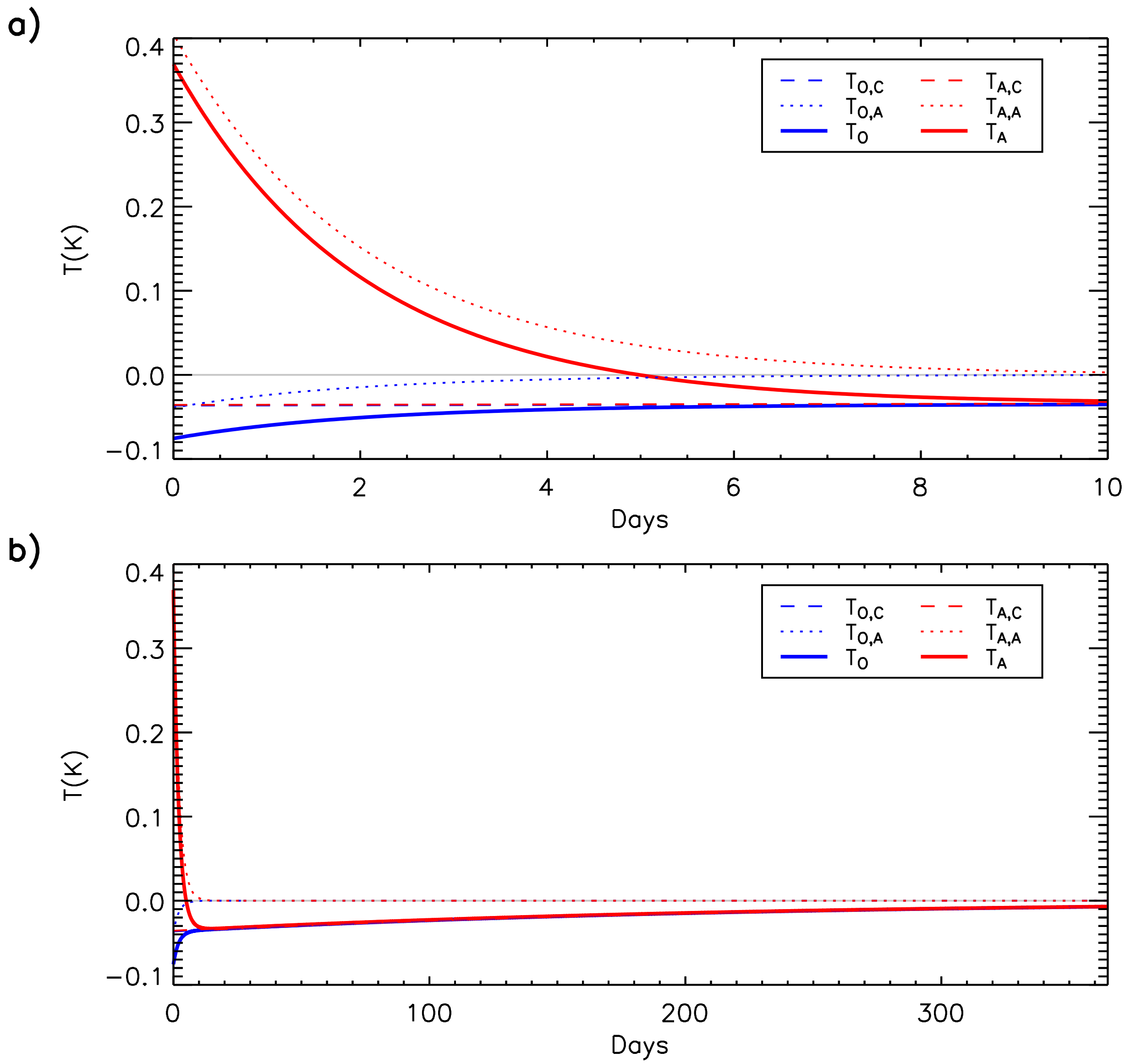

Fig. 9. Anomalous atmospheric (red) and ocean (blue) temperature during the first a) 10 days after the onset of forcing, and b) 500 days. The forcing consists of a single delta-function impulse applied for a single instant, equivalent to TOA forcing of -5 Wm^{-2} and surface forcing of -10 Wm^{-2} were both applied for one week. The total response is depicted by the heavy solid line. The ephemeral contributions of the atmospheric and coupled modes, proportional to $C_a \exp(-\lambda_a t)$ and $C_c \exp(-\lambda_c t)$ respectively, are given by the dotted and dashed lines.

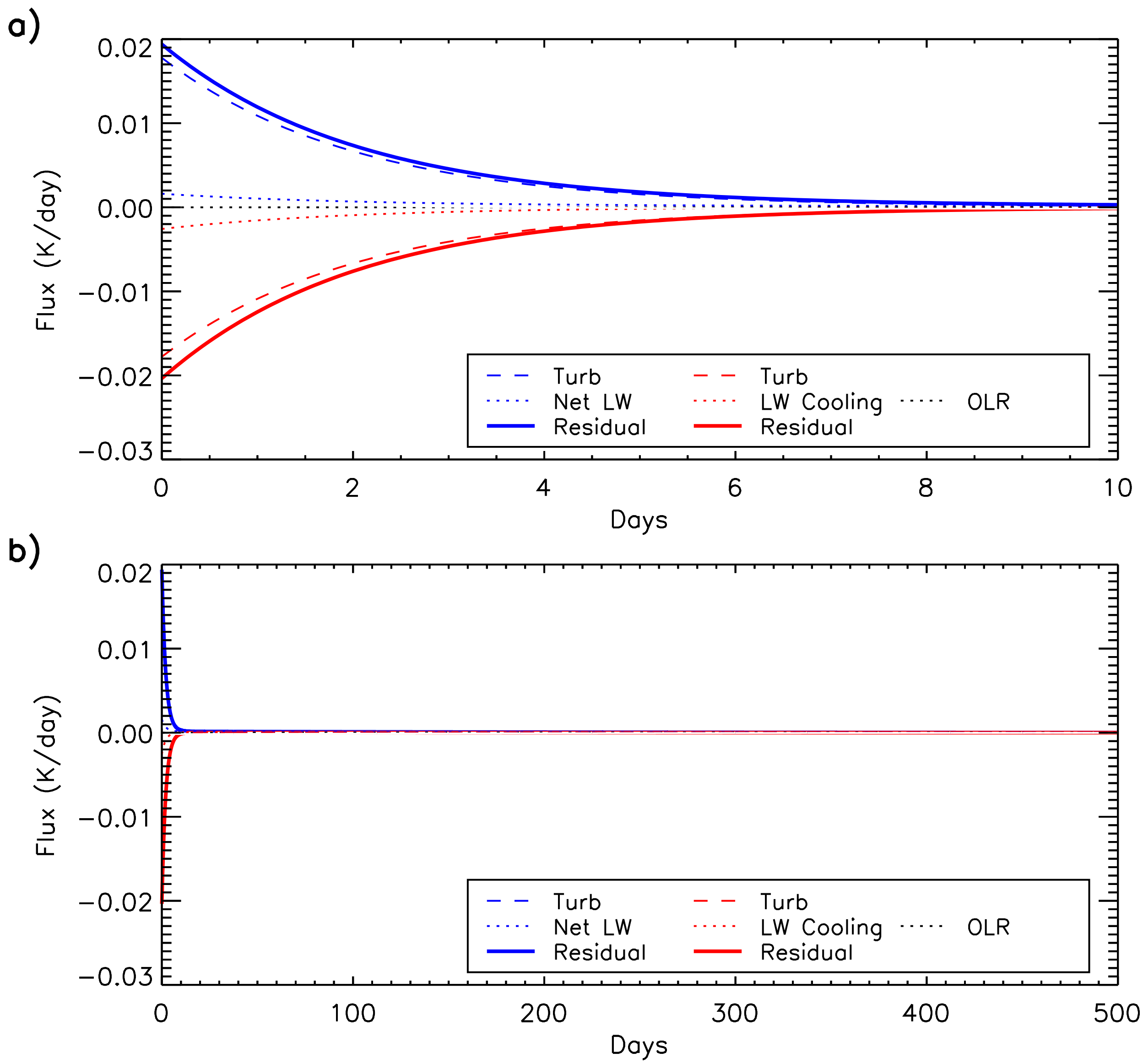

FIG. 10. Anomalous energy budgets corresponding to the anomalies in Figure 9 during the first a) 10 days after an isolated dust outbreak, and b) 500 days. In blue are fluxes comprising the surface energy budget according to (5): turbulent heat transfer from the atmosphere to the ocean (dashed), net longwave radiation (dotted), and their residual (thick solid). In red are the contributions to the atmospheric energy budget: turbulent heat transfer from the ocean to the atmosphere (dashed), net longwave cooling (dotted), and their residual (thick solid). In black, is the energy budget at the top of the atmosphere consistently solely of outgoing longwave radiation (dotted). All fluxes have units of K day^{-1}.

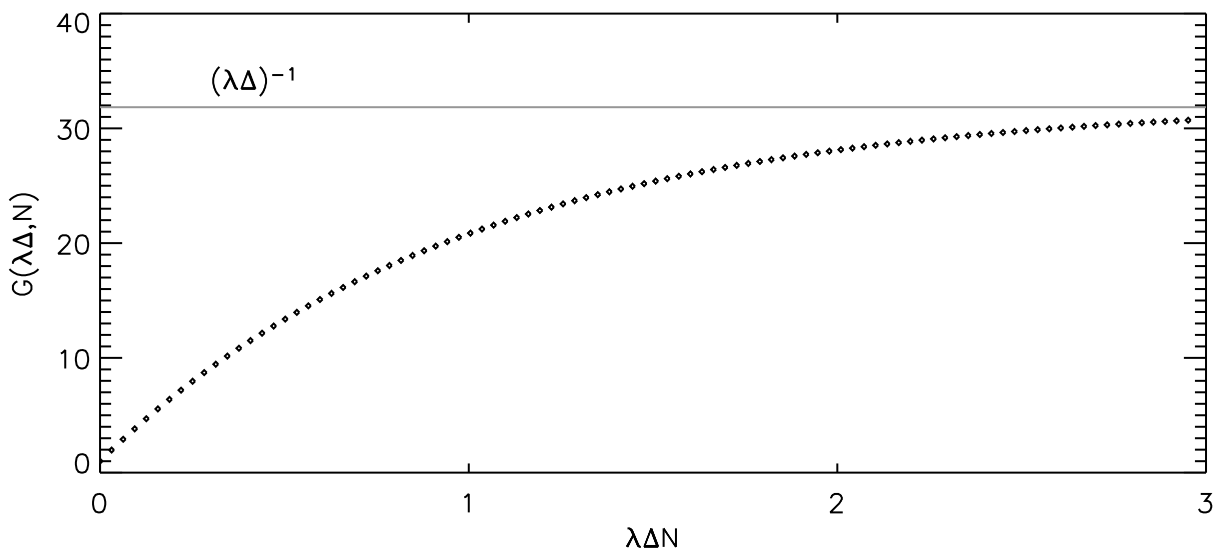

FIG. 11. The function $G(\lambda\Delta, N)$, representing the growing response to a succession of N dust outbreaks. Each dot corresponds to a single outbreak, which are separated in time by duration Δ (here, equal to one week). λ^{-1} gives the decay time scale of either the atmospheric or coupled mode. For this example, $\lambda^{-1} = 223\,$days, corresponding to the coupled mode. The gray, horizontal line is the asymptotic value $(\lambda\Delta)^{-1}$.

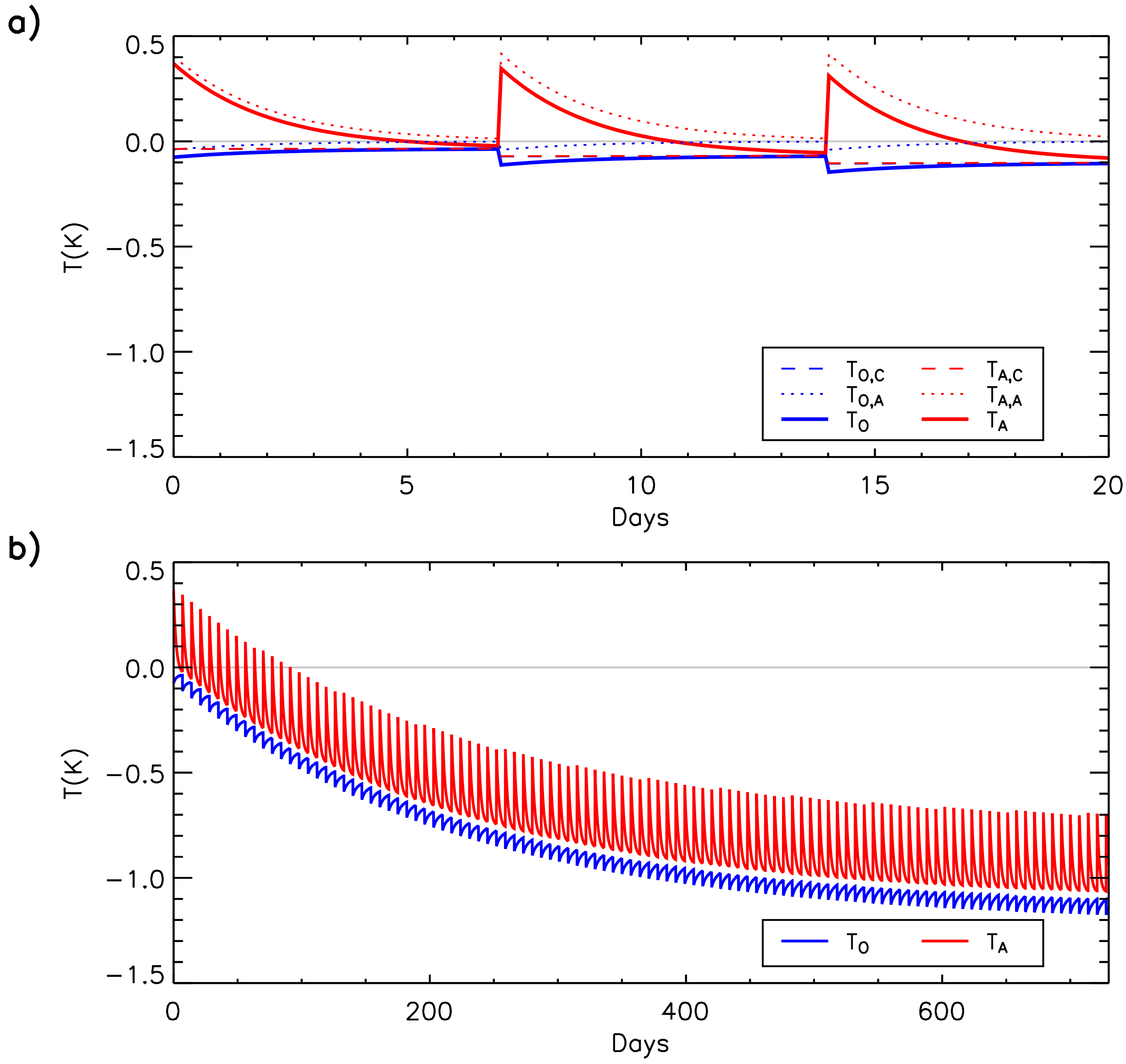

FIG. 12. As in Figure 9 but for a succession of dust outbreaks separated by a time interval $\Delta = 7$ days.

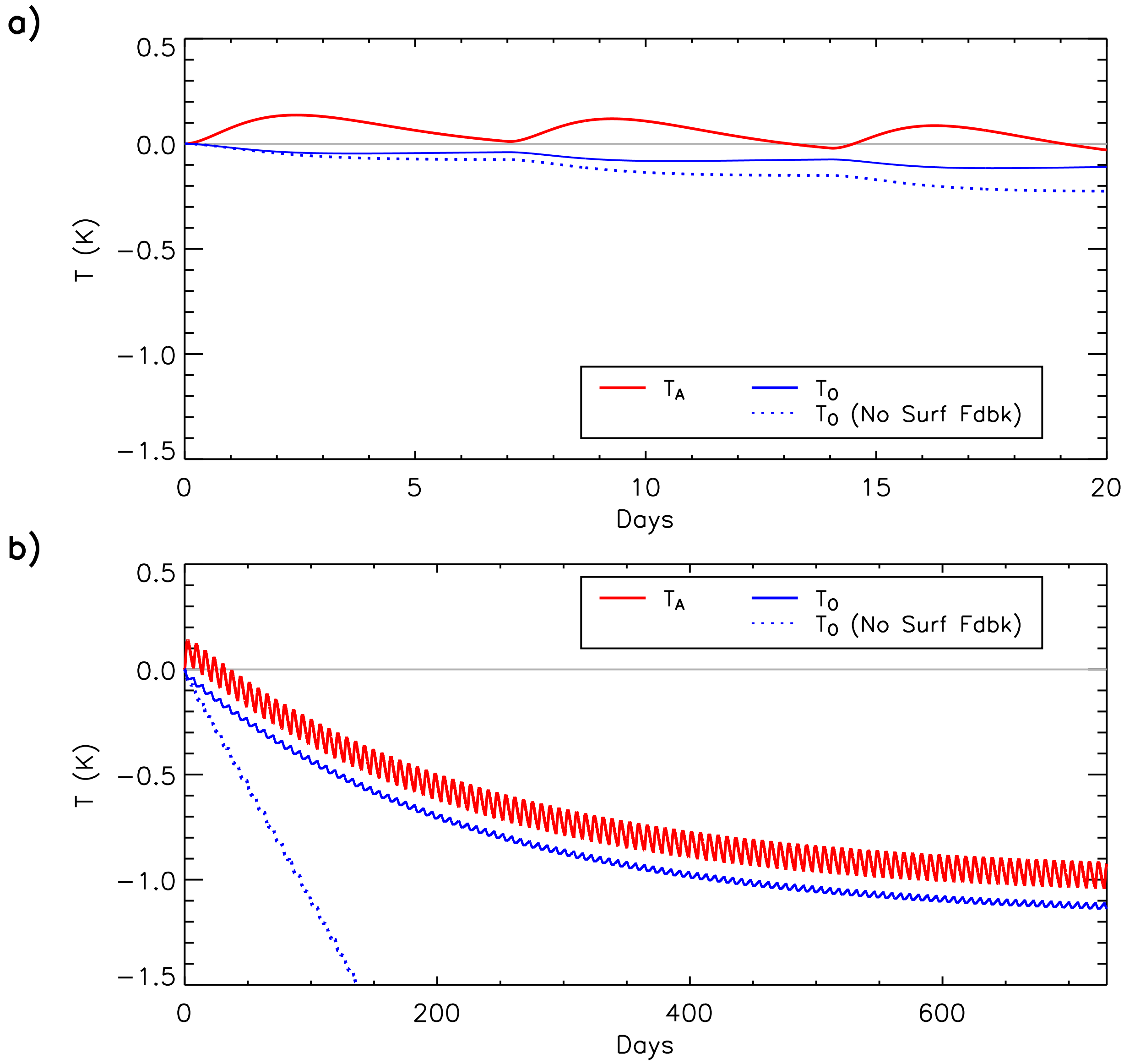

FIG. 13. As in Figure 12 but where the instantaneous forcing is replaced by forcing that is short-lived but of non-zero duration (and decays with a one-day e-folding time). The dotted line shows the ocean temperature response in the absence of coupling by the surface turbulent and radiative fluxes.

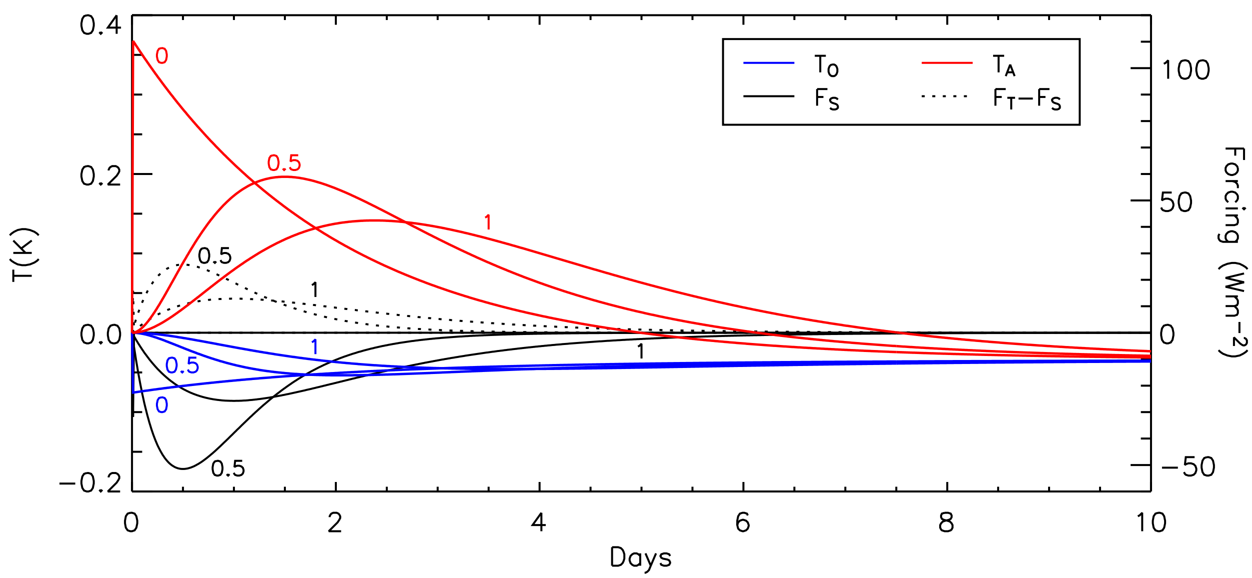

FIG. 14. Response during the first ten days to a single dust outbreak where the dust concentration and forcing increase gradually as described by (B9). The atmospheric and ocean temperature anomalies are shown in red and blue respectively. The atmospheric forcing (equal to the difference of the TOA and surface values) is depicted with a black dotted line, while surface forcing of the ocean is a black solid line. The response is shown for three different onset durations: $T = 0, 0.5$, and 1 days. For $T = 0$, the forcing is zero at all times except at $t = 0$.